

JGR Atmospheres

RESEARCH ARTICLE

10.1029/2020JD033811

Key Points:

- Identified fast, intermediate and slow transport pathways from various Northern Hemisphere surface regions into the Arctic
- Midlatitude tracers are transported via the fast and intermediate pathways while low latitude tracers are transported by the slow pathway
- Analyzed and quantified dynamical processes, such as transient versus mean transport, associated with different pathways

Supporting Information:

- Supporting Information S1

Correspondence to:

C. Zheng,
czheng@ldeo.columbia.edu

Citation:

Zheng, C., Wu, Y., Ting, M., Orbe, C., Wang, X., & Tilmes, S. (2021). Summertime transport pathways from different northern hemisphere regions into the Arctic. *Journal of Geophysical Research: Atmospheres*, 126, e2020JD033811. <https://doi.org/10.1029/2020JD033811>

Received 2 SEP 2020
 Accepted 22 JAN 2021

Author Contributions:

Conceptualization: Cheng Zheng, Yutian Wu, Mingfang Ting, Clara Orbe
Formal analysis: Cheng Zheng
Funding acquisition: Yutian Wu, Mingfang Ting, Clara Orbe
Investigation: Xinyue Wang
Methodology: Cheng Zheng, Yutian Wu, Mingfang Ting, Clara Orbe, Simone Tilmes
Project Administration: Yutian Wu, Mingfang Ting
Resources: Yutian Wu, Mingfang Ting
Software: Xinyue Wang, Simone Tilmes
Supervision: Yutian Wu, Mingfang Ting
Writing – original draft: Cheng Zheng

Summertime Transport Pathways From Different Northern Hemisphere Regions Into the Arctic

Cheng Zheng¹ , Yutian Wu¹ , Mingfang Ting¹ , Clara Orbe² , Xinyue Wang³ , and Simone Tilmes³ 

¹Lamont-Doherty Earth Observatory, Columbia University, Palisades, NY, USA, ²NASA Goddard Institute for Space Studies, New York, NY, USA, ³National Center for Atmospheric Research, Atmospheric Chemistry Observations and Modeling Laboratory, Boulder, CO, USA

Abstract Trace gases and aerosols play an important role in Arctic chemistry and climate. As most Arctic tracers and aerosols are transported from midlatitude source regions, long-range transport into the Arctic is one of the key factors to understand the current and future states of Arctic climate. While previous studies have investigated the air mass fraction and transit time distribution in the Arctic, the actual transport pathways and their underlying dynamics and efficiencies are yet to be understood. In this study, we implement a large ensemble of idealized tagged pulse passive tracers in the Whole Atmosphere Community Climate Model version 5 to identify and analyze summertime transport pathways from different Northern Hemisphere surface regions into the Arctic. Three different transport pathways are identified as those associated with fast, intermediate and slow time scales. Midlatitude tracers can be transported into the Arctic in the troposphere via the fast transport pathway (~8 days), which moves tracers northward from the source region mainly through transient eddies. For the intermediate transport pathway, which happens on 1–3 weeks' time scales, midlatitude tracers are first zonally transported by the jet stream, and then advected northward into the Arctic over Alaska and northern North Atlantic. Tropical and subtropical tracers are transported into the Arctic lower stratosphere via the slow transport pathway (1–3 months), as the tracers are lifted upward into the tropical and subtropical lower stratosphere, and then transported into the Arctic following the isentropic surfaces.

1. Introduction

The atmospheric composition of the Arctic, including trace gases and aerosols, has a substantial impact on Arctic climate and chemistry. Black carbon, which can be deposited onto ice and snow surfaces, or stay in the Arctic haze layer, increases the absorption of sunlight (e.g., Quinn et al., 2007; Warren & Wiscombe, 1980). The climate forcing due to black carbon is suggested to be twice as large as that of carbon dioxide (Hansen & Nazarenko, 2004) in the Arctic region. Long-wave radiative transfer over the Arctic can also be modulated by direct and indirect aerosol effects, as the microphysical properties of clouds can be affected by aerosols (Coopman et al., 2018; Garrett & Zhao, 2006; Lubin & Vogelmann, 2006). The production of tropospheric ozone in the Arctic, which acts as a greenhouse gas, is related to halocarbons originating from midlatitudes (Atlas et al., 2003; Klonecki et al., 2003). Studies have shown that the amount of aerosols (including black carbon) and trace gases (e.g., ozone precursors) in the Arctic is largely contributed by transport from sources in the midlatitudes and the tropics (e.g., Bottenheim et al., 2004; Fisher et al., 2010; Klonecki et al., 2003; Kupiszewski et al., 2013; Law & Stohl, 2007; Rahn and McCaffrey, 1980; Shindell, 2007; Shindell et al., 2008; Stohl, 2006). Thus, it is important to understand the long-range transport from lower latitudes into the Arctic.

The distribution of aerosols and tracer species in the Arctic is determined by multiple factors including emissions, chemistry, transport, and removal. The emissions, chemistry, and removal processes differ for different species, making it difficult to understand the distribution of tracers. At the same time, understanding the transport processes, especially from different parts of the globe into the Arctic, can provide useful information about the contribution to Arctic air masses from different source regions. One way to isolate transport processes from emissions or chemistry is to implement idealized passive tracers into a model. The idealized tracers, which have specified tracer removal time scales, are transported by the atmospheric flow in a model without active chemistry involved. Therefore, these idealized tracers highlight the

Writing – review & editing: Cheng Zheng, Yutian Wu, Mingfang Ting, Xinyue Wang, Simone Tilmes

advective-diffusive transport processes in the atmosphere, which are considered to be tracer-independent (e.g., Holzer & Hall, 2000; C. Orbe et al., 2012).

Previous studies have explored transport pathways into the Arctic using idealized tracers. C. Orbe, Newman et al. (2015a) investigated the Arctic airmass fractions using the Goddard Earth Observing System Chemistry-Climate Model, in which they used tracers subject to steady concentration boundary conditions over different regions in the planetary boundary layer (PBL) and then integrated the model to reach a statistical equilibrium state. At equilibrium, the concentrations of the tracers, therefore, reflected the fraction of air that last contacted the PBL in different source regions. These so-called Arctic “airmass fractions” therefore represented the relative contribution to Arctic tracer concentrations from different source regions. In particular, they found that the airmass in the Arctic lower troposphere is dominated by air that last contacted the PBL in the Arctic. By comparison, the air in the middle to upper troposphere of the Arctic mostly originates from Northern Hemisphere (NH) midlatitudes, with the primary contribution coming from the oceans during winter and from land during summer. Furthermore, they also showed that the airmass in the Arctic upper troposphere and lower stratosphere (UTLS) mainly originates from the tropics.

Using a related but distinct approach, Orbe et al. (2016) examined the transit-time distribution (TTD), derived from idealized pulse tracers, corresponding to transport from midlatitudes to the Arctic. Using the National Aeronautics and Space Administration (NASA) Global Modeling Initiative three-dimensional chemistry transport model, they found that during boreal summer, tracer concentrations in the Arctic upper troposphere peak around 10 days after the tracers are released, and the peak is around 30 days in the Arctic lower troposphere. The TTD described in Orbe et al. (2016) and the airmass fraction analysis in C. Orbe, Newman et al. (2015a) suggest that tracers released during summer in the midlatitudes are preferentially drawn upward across isentropic surfaces within the midlatitudes before being transported toward the Arctic approximately along the isentropes.

In this study, we focus on the summertime transport pathways into the Arctic by analyzing a large ensemble of passive pulse tracers (100 tracers), which is much larger than the four pulse tracers considered in Orbe et al. (2016), to achieve good statistics representing the summertime transport. Other studies have also shown the summertime transport into the Arctic and the impacts on Arctic climate using different approaches. For example, Laliberte and Kushner (2014) found that summertime midlatitude moisture, which can be transported into the Arctic, can explain a large part of the Arctic tropospheric temperature variability. Summertime black carbon concentrations over the Arctic, which mostly come from source regions at lower latitudes (e.g., D. Liu et al., 2015; Xu et al., 2017), can also have large impacts on radiative balance, which leads to increased warming in the Arctic (e.g., Bond et al., 2013; Hansen & Nazarenko, 2004). In addition, studies have also linked the Asian summer monsoon circulation to the climate and chemistry of the Arctic. Krishnamurti et al. (2015) examined a case study and argued that the moisture outflow associated with the Asian summer monsoon circulation caused a rapid melting of the Arctic sea ice during various monsoon heavy rainfall events in 2006–2012. H. Liu et al. (2003) also found that variability in the monsoon can lead to the variations in pollution transport into the Arctic. However, the role of the summer monsoon circulation on the Arctic transport is not well established. Note that the idealized tracers in our study, which have a spatially uniform source, are different from realistic tracer species that usually have large spatial variations in terms of their source or emission. Our approach with idealized tracers is to focus on the transport pathway, that is, how the idealized tracers are transported into the Arctic and what atmospheric circulation processes are involved. To attribute the Arctic concentration of any realistic chemical species to different source regions, an approach considering the spatial variation of the source distribution is required.

Several questions warrant further study in terms of summertime transport into the Arctic. First, what are the similarities and differences in transport pathways and timescales among different regions in the midlatitudes and the tropics? What are the physical processes involved in transporting tracers from the tropics and midlatitudes into the Arctic? As pointed out by Orbe et al. (2016), midlatitude tracers are preferentially lifted upward and then transported poleward during summer. To this end, we ask here: (a) What are the processes that lift up the tracers? By convection or large-scale rising motion? (b) What are the processes that transport the tracers northward into the Arctic? What is the relative importance of transient eddies and the mean atmospheric circulation? (c) How do the timescales and processes differ for different midlatitude regions? These questions will be the focus of this study. The model experimental design and diagnostic

methods will be introduced in Section 2. The evolution of tracer distribution in the Arctic will be discussed in Section 3. Different transport pathways, as well as the atmospheric circulations involved, will be explored in Section 4. Discussions and conclusions will be presented in Section 5.

2. Methods

2.1. Model Simulations

The whole atmosphere community climate model version 5 (WACCM5) is used in this study. WACCM5 is the high-top atmospheric component of the community earth system model version 1 (Hurrell et al., 2013). The WACCM5 used here has 110 vertical levels with a horizontal resolution of 0.9° latitude and 1.25° longitude. The model physics for WACCM5 is the same as the community atmospheric model version 5 (CAM5) (Neale et al., 2010), with the shallow convection scheme from S. Park and Bretherton (2009) and deep convection scheme developed by Zhang and McFarlane (1995). We integrate the model with prescribed historical sea surface temperatures and sea ice concentrations from January 1981 to December 1991.

The 110 vertical levels in WACCM5 greatly improve the vertical resolution from mid-troposphere to lower stratosphere (Garcia & Richter, 2019). The high-vertical resolution helps to better simulate the temperature, wind and water vapor distribution in the UTLS (Wang et al., 2018). Wu et al. (2020) used a similar setup of WACCM5 and found that the Asian summer monsoon region is favorable for fast transport of tracers from the surface into the UTLS. Thus, the 110-layer WACCM5 can be beneficial for understanding the tracer transport within the UTLS and from Asian summer monsoon region to the Arctic (e.g., Ikeda et al., 2017; Koch & Hansen, 2005).

2.2. Idealized Tracers

The idealized tracers imposed in the model are similar to that in Wu et al., (2020). Here, we use the “boundary impulse response (BIR),” or simply “pulse” tracer approach (Haine et al., 2008; Holzer et al., 2000). The BIR can be interpreted as the time-evolving response $G(r, t | \Omega, t')$ at a location r and time t to a pulse of a conserved and passive tracer which is released in the source region Ω at time t' . BIR is tracer-independent as it does not involve any chemical processes or interior sources/sinks (e.g., Holzer & Hall, 2000; C. Orbe et al., 2012). Therefore, the BIR provides a direct measure of transport properties from source regions into the Arctic, which isolates the transport from chemistry processes. This approach has been used to examine seasonal variations in stratospheric age spectra (F. Li et al., 2012; Ploeger & Birner, 2016), transport from the NH midlatitude surface to different regions around the globe (Orbe et al., 2016), as well as transport from NH surface to UTLS (Wu et al., 2020). Note that the BIR can be used to construct the TTD, which is one approach used in previous studies (Holzer & Hall, 2000; F. Li et al., 2012; Orbe et al., 2016) to measure the transit time at r independent of when (with respect to t') the tracer was last at the Earth's surface. Similar to Wu et al. (2020), our focus here is on quantifying how the tracer distribution at time t and location r is related to tracer source Ω conditioned on its release time.

Idealized pulse tracers are imposed in WACCM5 over different NH surface regions. The regions are shown in Figure 1a. There are 5 NH midlatitude regions, including Asia (ASI), Pacific (PAC), North America (NAM), Atlantic (ATL), and Europe (EUR). The northern boundary of these regions is located at 60°N and the southern boundaries range from 20° to 25°N , which are similar to that in C. Orb, Newman et al. (2015a). In addition, to highlight the role of the Asian summer monsoon, we also tagged tracers that are released over the Tibetan Plateau (TP) and North India (NI). Tracers that are released to the south of these regions in NH are tagged as Tropics (TR). Note that although we also release tracers north of 60°N , we will not include this case here as our focus is on long-range transport pathways into the Arctic. Tracers are released uniformly at each source region during the first day. The tracer concentration is set to 1 mol/mol at the surface during the first 24 h within the source region, while outside the source region the boundary concentration is set to 0. The tracers are transported freely in the atmosphere with no loss as long as they do not touch the surface. The tracer concentration is set to 0 whenever they are in contact with the surface after the first day. The transport of pulse tracers into the Arctic, which can happen on relatively short time scales, likely have a high dependency on meteorology. Thus, large variability in the transport is expected from tracer to tracer when they are released at different times. To achieve more robust results, a large ensemble of tracers

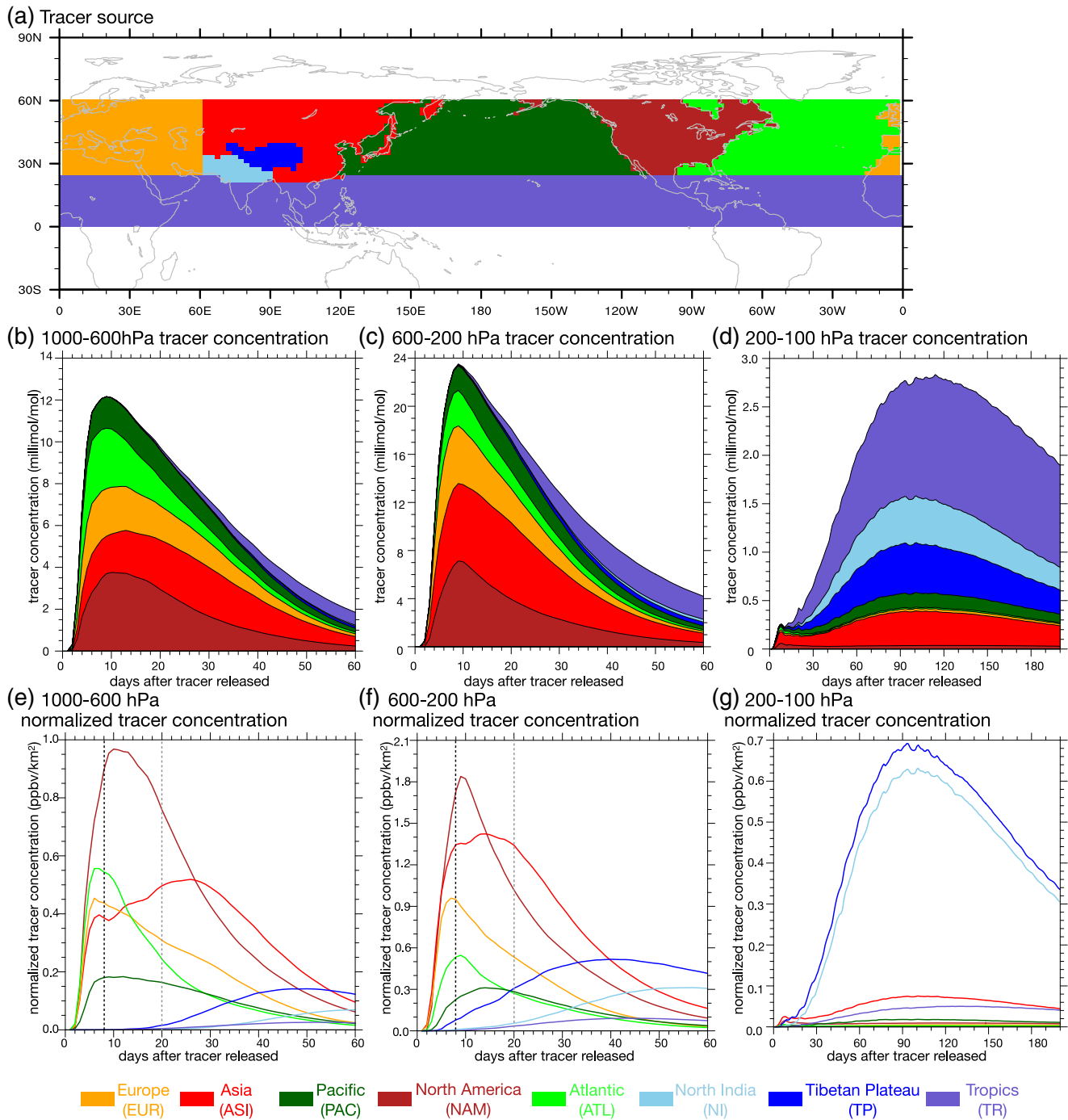


Figure 1. a) Definition of the source regions for EUR, ASI, PAC, NAM, ATL, NI, TP, and TR tracers. (b–d) Temporal evolution of tracer concentration in the Arctic (north of 70°N) at 1,000–600 hPa, 600–200 hPa, and 200–100 hPa, respectively. Each color shading represents tracers that are released in one region. Tracer concentration is multiplied by 1,000. Unit in millimole/mole. (e–g) Temporal evolution of normalized tracer concentration in the Arctic at the same pressure levels in (b–d). Unit in ppbv/km². The tracer concentration is divided by the area of the source region as the tracer concentration is normalized (also see main text). The dashed black lines and dashed gray lines denote day 8 and day 20 after the tracers are released respectively in (e–f). ASI, Asia; ATL, Atlantic; EUR, Europe; NAM, North America; NI, North India; PAC, Pacific; TR, Tropics; TP, Tibetan Plateau.

is implemented in the model. A total of 10 tracers are released each summer, on days 3, 10, 17, 24, and 31 in July and August, and repeated for all 10 summer seasons, 1981–1990. Therefore, we have a total of 100 tracers for each source region. The choice of 100 tracers for each source region is a compromise between maximizing the number of tracer ensembles and the computational costs of the model experiments. Model outputs of daily means of meteorological fields, as well as tracer concentrations and budget terms, are saved for further analysis. Compared to Orbe et al. (2016), with a much larger number of tracers (100 vs. 4) and multiple midlatitude regions, the methods used in this study can provide information that potentially links the Arctic tracer concentration to different NH source regions, as well as decomposes the transport into transients and time-mean components (see Section 2.3).

2.3. Diagnostics of Tracer Transport

The daily model output is interpolated to 28 pressure levels from 1,000 to 50 hPa prior to any analysis. The intervals among the pressure levels are 50 hPa from 1,000 to 300 hPa, 25 hPa from 300 to 100 hPa, and 10 hPa from 100 to 50 hPa. As in Wu et al. (2020), the tracer budget can be written as the contribution from different processes:

$$\frac{\partial \chi}{\partial t} = \text{RD} + \text{VD} + \text{COND} + \text{CONS}, \quad (1)$$

where χ is the concentration of the pulse tracer. RD, VD, COND, and CONS are the tracer tendencies due to transport by model's resolved dynamics, vertical diffusion, deep convection and shallow convection, respectively. The tracer concentration χ , as well as the four terms on the rhs of (1) are all taken from the direct model outputs. Wu et al. (2020) showed that Equation 1 is well-balanced by using the model outputs, and the balance is also well maintained after the data are interpolated onto pressure levels (not shown). The transport of the tracers by resolved dynamics RD is simply the advection of the tracers by the model's (resolved) circulation:

$$\text{RD} = -\vec{U} \cdot \nabla \chi, \quad (2)$$

where \vec{U} is the three-dimensional wind vector. In the pressure coordinates, as the divergence of the three-dimensional wind is zero ($\nabla \cdot \vec{U} = 0$), (2) can be written as:

$$\text{RD} = -\nabla \cdot (\vec{U} \cdot \chi), \quad (3)$$

or,

$$\text{RD} = -\frac{\partial(u \cdot \chi)}{\partial x} - \frac{\partial(v \cdot \chi)}{\partial y} - \frac{\partial(\omega \cdot \chi)}{\partial p}, \quad (4)$$

where u , v , and ω are zonal, meridional and vertical motion in pressure coordinates. Therefore, the tracer tendency due to resolved dynamics equals the convergence of the three-dimensional tracer flux by the resolved atmospheric circulation. As daily χ , u , v , and ω are available, we can compute the contributions of tracer tendency by resolved dynamics in the zonal, meridional and vertical directions explicitly. Note that model output RD is calculated on the model grid (hybrid vertical levels) at each model time step, while we estimate each term on the rhs of Equation 4 by using daily mean values on pressure levels. Therefore, the estimation using the rhs of Equation 4 may contain some errors, which will be discussed in Section 4.

When computing the tracer tendency using Equations 1 and 4, we will only show the results for the ensemble mean of tracers, as tracer to tracer variability is not the focus of this study. However, tracer to tracer variability can provide information regarding the contributions from time-mean and transient flows. We analyze the variability from tracer to tracer by considering the time series of the tracer concentration. Given N number of tracers that are released at $t' = t'_1, t'_2, \dots, t'_N$ and at source region Ω , the tracer concentration of one particular tracer (n) at location r at a fixed transit time (number of days after the tracers are released) $\xi = t - t'$ (where t is the current time when the tracer concentration is observed) can be written as:

$$\chi(n, \xi, \Omega, r),$$

where $n = 1, 2, \dots, N$. As t' is only a function of n , and time $t = \xi + t'$, for fixed transit time ξ , t and n is an injective function (one-to-one function). So, $\chi(n, \xi, \Omega, r)$ can also be written as.

$$\chi(t(n, \xi), \xi, \Omega, r)$$

which can be considered as a time series. Note that the method here to consider an ensemble of pulse tracers that are released at different time as a time series at fixed transit time ξ , is the same as the method used in Holzer et al. (2003). This time series can be decomposed into the time mean (averaging over t) and the deviation from time mean:

$$\chi(t(n, \xi), \xi, \Omega, r) = \bar{\chi}(\xi, \Omega, r) + \chi'(t(n, \xi), \xi, \Omega, r),$$

here the overbar denotes the time mean, and prime denotes the deviation from the time mean. Again, for fixed transit time ξ , t and n is an injective function (one-to-one function), so averaging over t is equivalent to averaging over n . Thus, the time mean $\bar{\chi}(\xi, \Omega, r)$ is equivalent to ensemble mean of tracers at fixed ξ .

Similarly, the time series of circulation variables, such as the meridional wind $v(t, r)$ can also be decomposed in a similar way:

$$v(t(n, \xi), r) = \bar{v}(\xi, r) + v'(t(n, \xi), r),$$

To match the form of tracer concentration, both the time-mean meridional wind and the deviation from time mean also depend on transit time ξ . Thus we can write the time mean of the meridional flux of tracers as

$$\overline{v \cdot \chi} = \bar{v} \bar{\chi} + \overline{v' \chi'}, \quad (5)$$

where the first term on the rhs of Equation 5 is the transport by time-mean meridional wind (including both zonal mean meridional circulation and stationary waves), and the second term represents the transport by transients that includes all time scales shorter than the time mean.

Similar to Equation 5, the vertical flux of the tracer transport by resolved dynamics can be decomposed as:

$$\overline{\omega \cdot \chi} = \bar{\omega} \bar{\chi} + \overline{\omega' \chi'}. \quad (6)$$

To evaluate the relative contribution from time-mean and transient components.

The analysis in this study will only focus on the ensemble mean of 100 tracers for each source region, which are released during July and August in 10 years. That means we only investigate the transport pathways in terms of climatological mean. Different transport pathways can have subseasonal, interannual, and decadal variabilities, which are beyond the scope of this study and will be explored in the future.

3. Temporal Evolution of Tracer Concentration in the Arctic

We focus on the tracer concentration in the Arctic, which is defined as the region north of 70°N. When the pulse tracers are released, sharp horizontal gradients of tracer concentration are created at the boundaries of the tracer source regions (e.g., the northern boundary of midlatitude source regions at 60°N in Figure 1a). These sharp gradients can lead to artificially strong horizontal transport of tracers locally due to diffusion or mixing (also see Section 4.2). Thus, the southern boundary of the Arctic is defined as 70°N, away from the northern boundary of the source regions (60°N). The time evolution of tracer concentration for lower-to-mid troposphere (1,000-600 hPa), mid-to-upper troposphere (600-200 hPa), and lower stratosphere

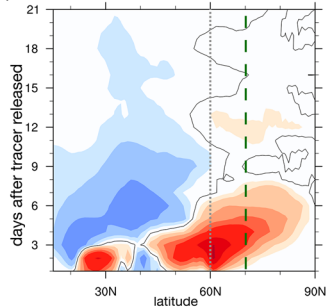
(200–100 hPa) over the Arctic is shown in Figures 1b–1d, respectively. Each color denotes the contribution from one source region. The total tracer concentration from all source regions peaks at about 10 days in the troposphere (Figures 1b and 1c), but at around 100–120 days in the lower stratosphere (Figure 1d). In the troposphere, most of the Arctic tracers originate from the five midlatitude regions: ASI, PAC, NAM, ATL, and EUR on relatively short time scales. Tracers from the tropics only contribute significantly after days 20–30 from the day the tracers are released. In the lower stratosphere, most of the contribution to the Arctic tracer concentration is from the tropics, as well as TP and NI tracers, with ASI tracers having the largest contribution among the five midlatitude regions. The Asian summer monsoon regions (TP and NI), which cover a relatively small area compared to the tropical region TR (Figure 1a), have significant contributions to the tracer concentration in the Arctic lower stratosphere (Figure 1d), showing that TP and NI tracers are transported into the Arctic lower stratosphere very efficiently. Note that, these findings are consistent with the results in C. Orbe, Newman et al. (2015a), in that most of the tracer concentration over the Arctic troposphere originates from the midlatitudes, whereas the tropics has the largest contribution to the tracer concentration in the Arctic lower stratosphere. However, our results cannot be quantitatively compared to C. Orbe, Newman et al. (2015a) as the tracers are removed when they come in contact with the surface after day 1, whereas tracers are retagged in C. Orbe, Newman et al. (2015a) when they touch the surface. In addition, since a large number of tracers are removed at the surface (see Section 4.2), only a small portion of the tracers are transported into the Arctic. As tracer species and aerosols are not necessarily removed when they touch the surface in the real atmosphere, it is not very meaningful to quantify the exact tracer fraction that are, transported into the Arctic in our experiment.

As the areas covered by different source regions differ, to better compare the efficiency of the tracer transport from different regions, we normalized the tracer concentration by the area of the source region. The normalized tracer concentration, which is measured by the Arctic tracer concentration (ppbv) per unit area of source region (square kilometer), is shown in Figures 1e–1g. Among the five midlatitude regions (ASI, PAC, NAM, ATL, and EUR) that have most of the contributions to the Arctic tracer concentration in the troposphere, ATL, EUR, and NAM tracers have sharp peaks with fast growth and decay: ATL and EUR tracers peak at around 6–9 days in both lower and upper troposphere while NAM tracers at about 10 days. In comparison, ASI and PAC tracers have flat peaks. Both ASI and PAC tracer concentration stays in high value during day 10–20 in mid-to-upper troposphere (Figure 1f). ASI tracer concentration slowly increases during day 10–30 in the lower troposphere, while PAC tracer concentration slowly decreases during day 10–20 (Figure 1e). The growth rate of the tracer concentrations in the Arctic troposphere (the slope of the normalized concentrations in Figures 1e and 1f) is the largest during the first 6–8 days for ASI, PAC, ATL, and EUR tracers, indicating that similar dynamical processes are likely at play on the short timescales in these regions. We name this the fast transport pathway. From days 8–20, the tracer concentrations tend to maintain at high values in the mid-to-upper troposphere for ASI and PAC tracers (Figures 1e and 1f). This will be referred to as the intermediate transport pathway with a timescale of about 1–3 weeks. For NAM tracers, the peak time is about 10 days, which is shorter than ASI and PAC and longer than EUR and ATL. Later on, we will show that this is likely due to the combination of the fast and intermediate transport pathways.

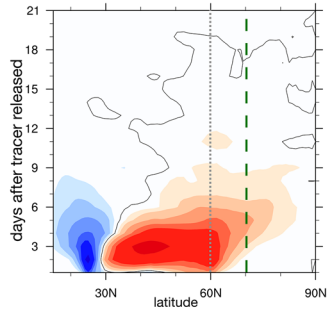
For the Arctic lower stratosphere, although TR has the largest contribution to the total concentration (Figure 1d), NI and TP tracers are more efficiently transported into the Arctic when normalized by the surface areas, compared to other regions, with a peak time around 90–100 days (Figure 1g). The growth rate of the NI and TP tracers becomes large at about 20 days after the tracers are released. This indicates the important role the Asian summer monsoon plays in tracer transport into the Arctic lower stratosphere (C. Orbe, Waugh et al., 2015). ASI and TR tracers are also transported into the Arctic on the 100-days to 150-days time scales, while the transports from ATL, PAC, EUR, and NAM are negligible on the long time scales. It is interesting to note that the 100-days time scale is much longer than that within the troposphere (Figures 1e and 1f). This will be termed as the slow transport pathway in the rest of the study.

The three different transport pathways noted above, with fast (~1 week), intermediate (1–3 weeks) and slow (1–3 months) time scales, are defined by analyzing the evolution of the passive tracer concentration reaching the Arctic. In the real atmosphere, different tracer species have different lifetimes. For example, the lifetime of butane is about 1 week, propane has a lifetime of about 2 weeks, and ethane and carbon monoxide have averaged lifetimes of approximately 2 months. Thus, the three transport pathways may play

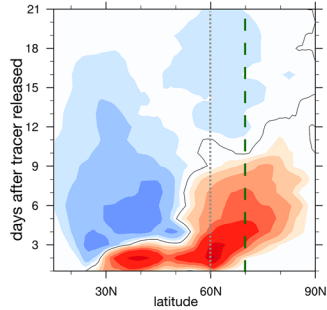
(a) zonal and vertical averaged $\bar{v} \cdot \bar{\chi}$ for ASI



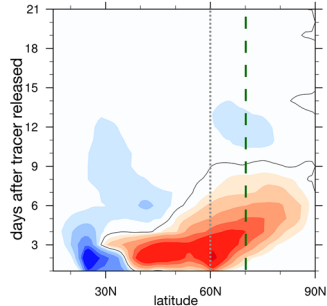
(b) zonal and vertical averaged $\bar{v} \cdot \bar{\chi}$ for PAC



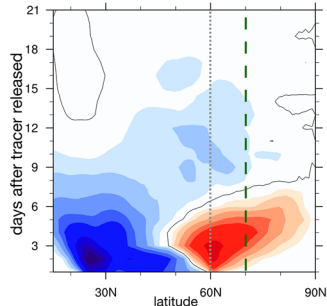
(c) zonal and vertical averaged $\bar{v} \cdot \bar{\chi}$ for NAM



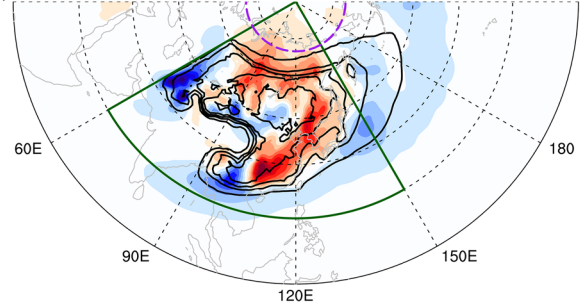
(d) zonal and vertical averaged $\bar{v} \cdot \bar{\chi}$ for ATL



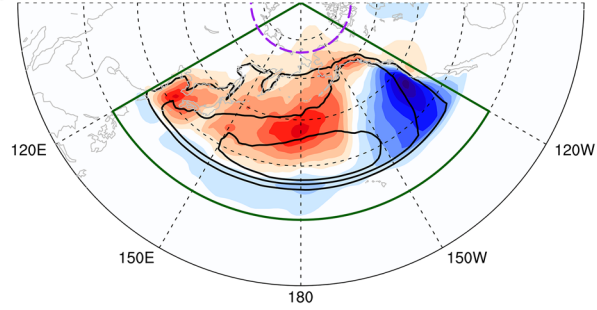
(e) zonal and vertical averaged $\bar{v} \cdot \bar{\chi}$ for EUR



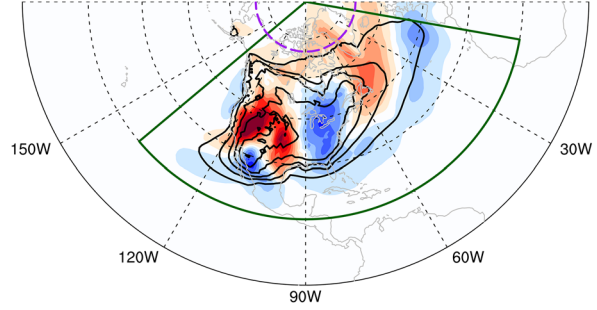
(f) Day 1-8 vertical averaged $\bar{v} \cdot \bar{\chi}$ for ASI



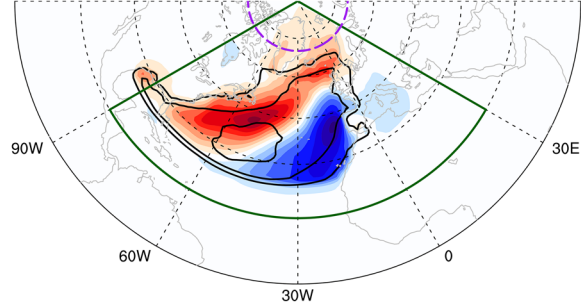
(g) Day 1-8 vertical averaged $\bar{v} \cdot \bar{\chi}$ for PAC



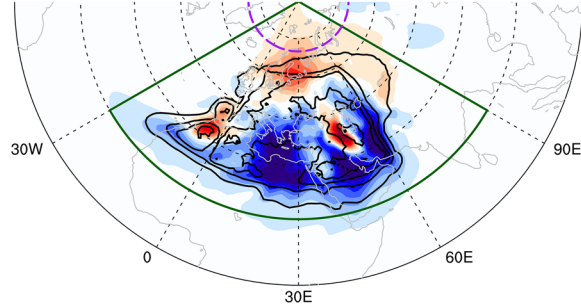
(h) Day 1-8 vertical averaged $\bar{v} \cdot \bar{\chi}$ for NAM



(i) Day 1-8 vertical averaged $\bar{v} \cdot \bar{\chi}$ for ATL



(j) Day 1-8 vertical averaged $\bar{v} \cdot \bar{\chi}$ for EUR



different roles in transporting different tracer species. For example, the slow transport pathway may have little contribution to short-lived species like butane and propane; while the fast transport pathway may be relevant for tracer species of both short and long lifetimes. Note that these examples are just used to illustrate that different pathways can be potentially important for different tracer species. However, as our experimental design does not consider tracer loss via certain processes (e.g., wet deposition, which can happen when tracer species are rained out), as such, it cannot completely address the question of the relevance of different transport pathways for any specific tracer species. In the following sections, we will explore the dynamical processes contributing to each of the three transport pathways by using actual concentration of the tracer (not normalized concentration).

4. Tracer Transport Pathways Into the Arctic

4.1. The Role of Meridional Tracer Flux

Before going into details of the different transport pathways, we first consider the budget of the tracer concentration integrated over all grid points in the Arctic ($\iiint_{\text{arctic}} \chi$), from the surface to the top of the atmosphere and from 70°N to the north pole. Using tracer mass conservation, one can show that the budget of the total Arctic tracer concentration ($\iiint_{\text{arctic}} \chi$) can be written as:

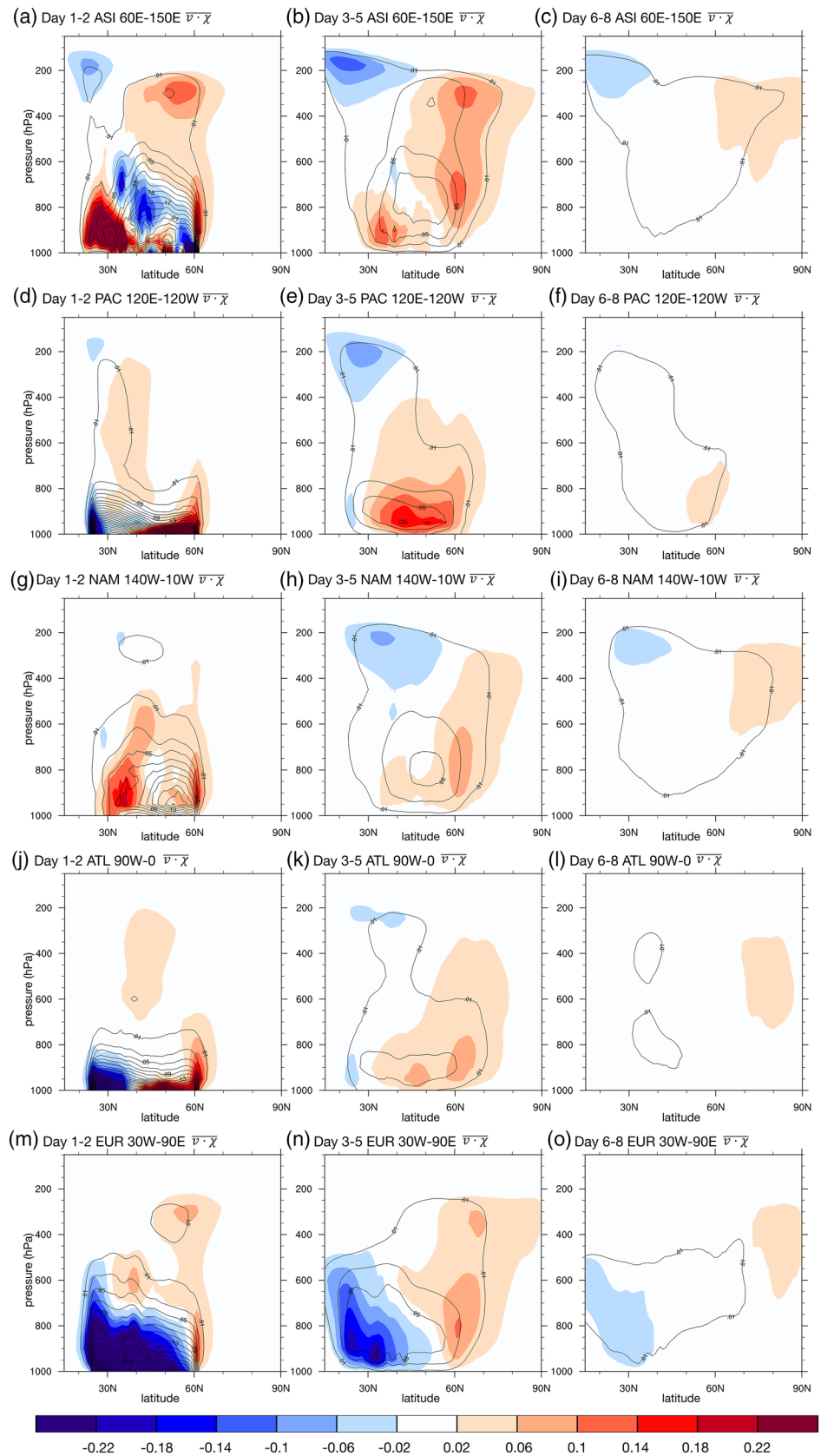
$$\frac{\partial}{\partial t} \iiint_{\text{arctic}} \chi dV = \oint_{70^{\circ}\text{N}} v \cdot \chi + (\text{removal of tracer at Arctic surface}). \quad (7)$$

Thus, the only way tracers can be transported into the Arctic from the midlatitudes or tropics is through the poleward flux at the southern boundary, that is, 70°N. The temporal and spatial distribution of the meridional flux can thus determine the evolution of the tracer concentration within the Arctic. To illustrate this, we show the vertically (1,000–100 hPa) and zonally averaged meridional flux of the five midlatitude regions (ASI, PAC, NAM, ATL, and EUR) in Figures 2a–2e. The strongest poleward flux at 70°N (dark green dashed line) is within the first 8 days for all five regions. This is consistent with the largest growth rate of tracer concentration during the first 8 days in Figures 1e–1f (the fast transport pathway; see Section 3), as implied by Equation 7. The meridional flux shifts to negative (black line indicates the zero line) after about day 7–9 for ATL and EUR tracers, corresponding to the decrease of tracer concentration after 7–9 days (Figures 1e and 1f); the meridional flux stays positive with a small amplitude from about day 8–20 for ASI and PAC tracers, which is also consistent with the tracer evolution during that period of time (Figures 1e and 1f; the intermediate transport pathway). In addition, the meridional tracer flux shifts to negative at around day 10 for NAM tracers, which coincides with the timing of the peak tracer concentration of NAM tracers (Figures 1e and 1f). Therefore, the key to explain the tracer evolution within the Arctic is to understand the spatial and temporal structure of the meridional tracer fluxes, which will be the main focus in the following discussions about the fast and intermediate transport pathways.

4.2. The Fast Transport Pathway

As discussed above, the meridional tracer flux is large during the first 8 days after the tracers are released for all the midlatitude source regions. We show in Figures 2f–2j, the spatial structure of the vertically integrated meridional tracer flux (shading in Figure 2) for ASI, PAC, NAM, ATL, and EUR. The vertically integrated tracer concentrations, denoted by the black contours, show the highest concentration located near where

Figure 2. a) Zonally and vertically (1,000–100 hPa) averaged tracer meridional flux at different latitude (15°N–90°N) and different time (1–21 days) after the ASI tracers are released. The black contour denotes the zero line and the dashed dark green line marks the boundary of the Arctic region (70°N). The dashed gray line denotes the northern boundary of the tracer source region. Unit of the meridional flux is in $(\text{mol} / \text{mol}) \cdot (\text{m} / \text{s})$. (b–e) The same as (a), but for PAC, NAM, ATL, and EUR tracers, respectively. (f) The shadings are vertically averaged (1,000–100 hPa) tracer meridional flux during day 1–8 for the ATL tracers. Unit in $(\text{mol} / \text{mol}) \cdot (\text{m} / \text{s})$. Black contour lines show the vertically averaged (1,000–100 hPa) ASI tracer concentration during day 1–8. The contour interval is 0.01 mol/mol. Dashed purple line denotes the boundary of the Arctic region (70°N). (g–j) The same as (f), but for PAC, NAM, ATL, and EUR tracers, respectively. In (f–j), the regions defined by the dark green line are where further analysis will be performed in Figures 3–5. The southern boundaries are at 15°N while the northern boundaries are at 90°N. The east and west boundaries are 60°E–150°E in (f), 120°E–120°W in (g), 140°W–10°W in (h), 90°W–30°E in (i), and 30°W–90°E in (j). ASI, Asia; ATL, Atlantic; EUR, Europe; NAM, North America; NI, North India; PAC, Pacific; TR, Tropics; TP, Tibetan Plateau.



the tracers are released. Northward flux into the Arctic is located in regions directly to the north of each source region. This indicates that the fast transport pathway is mostly due to direct northward transport from the source region into the Arctic by the atmospheric circulation.

To determine the vertical structure of the meridional transport, Figure 3 shows the zonally averaged tracer concentration and meridional flux over the local area outlined by the dark green lines as in Figure 2 for each region. These cross sections are plotted for days 1–2, 3–5, and 6–8 after the tracers are released for ASI, PAC, NAM, ATL, and EUR tracers to better illustrate the temporal evolution.

There are some similarities among the cross sections for tracers released in different midlatitude regions. During day 1–2 (first column in Figure 3), strong northward transport can be found near 60°N in the lower troposphere among all regions. As the northern boundary of the tracer source regions is at 60°N, a strong meridional gradient of tracer concentration appears immediately after the tracers are released. The maximum northward flux of tracers at 60°N in the lower troposphere is expected (first column in Figure 3 and first column in Figure 2). In addition, the northward transport in the upper troposphere is broader and weaker compared to the lower troposphere during day 1–2. The tracer concentration (black contours) is higher in the lower troposphere than in the upper troposphere, but a small amount of tracers have already been lifted up into the upper troposphere during day 1–2. During day 3–5 (second column in Figure 3), compared with day 1–2, the northward flux extends northward, with large northward transport in both upper and lower troposphere. Although the tracer concentration generally decreases during day 3–5 due to the surface removal process, the concentration is more evenly spread out in the vertical, indicating further lifting of lower tropospheric tracers into the upper troposphere. Both the tracer concentration and the northward flux become weaker during day 6–8 (third column in Figure 3).

The northward flux going into the Arctic is the strongest during day 3–5, with strong transport in both the upper and lower troposphere among all five regions. The question is what processes are responsible for the upward tracer transport from the surface into the lower and upper troposphere. We apply the tracer budget analysis as in Equations 1 and 4 to address this question. The different terms on the right side of Equation 1 are shown in Figure 4 averaged for 30°–70°N region as in Figure 3, for the upper (200–500 hPa; first column) and lower troposphere (500–950 hPa; second column). Following Equation 1, the tendency of the tracers can be separated into contribution from deep convection (COND; red), shallow convection (CONS; orange), vertical diffusion (VD; blue), and resolved dynamics (RD; green). With Equation 4, the resolved dynamics term can be further decomposed into transport by zonal wind (purple), meridional wind (magenta), and vertical velocity (cyan). The three-dimensional decomposition of the transport by resolved dynamics is crosshatched to distinguish them from the four terms in Equation 1. The sum of the three-dimensional convergence components is approximately equal to the resolved dynamics term, as the residual (yellow shadings) is generally small. Note that the results for all five midlatitude regions are qualitatively similar in Figure 4. During days 1–2 in the upper levels (Figure 4a), deep convection (red) has the largest contribution. There is also significant contribution from resolved dynamics (green), which mostly comes from the vertical transport (crosshatched cyan). For days 3–5 in the upper troposphere (Figure 4c), there is little contribution by diffusion or convection processes (COND, CONS, and VD). Instead there is a large positive tracer tendency due to vertical transport by resolved dynamics, while at the same time, the tracers are also transported out of the region by zonal and meridional fluxes. For days 6–8, the tracer tendency in the upper levels is mostly from the zonal transport, which is transported downstream out of the averaging region. In summary, tracers are transported into the upper troposphere mostly by deep convection and resolved dynamics (specifically, vertical fluxes). If we combine the contribution during both days 1–2 and 3–5, the net effect of vertical transport by resolved dynamics is comparable to the contribution by deep convection in all five regions.

Figure 3. a) Meridional and vertical structure of tracer meridional flux and concentration during day 1–2 for ASI tracers. The shadings are meridional flux of ASI tracers averaged over 60°E–150°E (the region denoted by dark green line in Figure 2f). Unit in $(\text{mol} / \text{mol}) \cdot (\text{m} / \text{s})$. The contours are tracer concentration averaged also over 60°E–150°E. The contour lines start from 0.01 mol/mol, with an interval of 0.02 mol/mol. (b–c) The same as (a), but for day 3–5 and 6–8. (d–f) The same as (a–c) but for PAC tracers. The averaging is performed over 120°E–120°W (also see Figure 2g). (g–i) The same as (a–c) but for NAM tracers. The averaging is performed over 140°W–10°W (also see Figure 2h). (j–l) The same as (a–c) but for ATL tracers. The averaging is performed over 90°W–30°E (also see Figure 2i). (m–o) The same as (a–c) but for EUR tracers. The averaging is performed over 30°W–90°E (also see Figure 2j). ASI, Asia; ATL, Atlantic; EUR, Europe; NAM, North America.

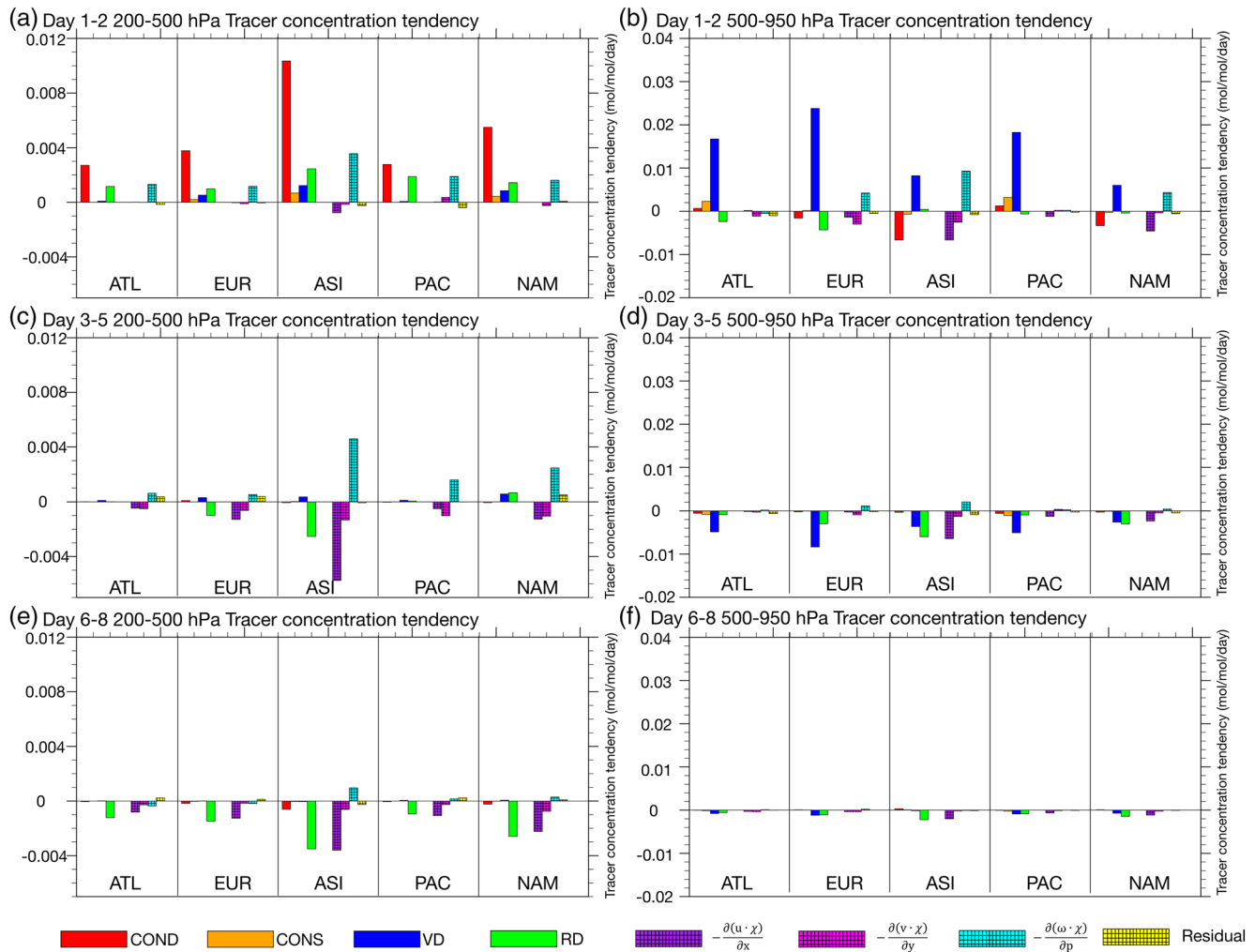


Figure 4. a) Tracer budget analysis during day 1–2 in the upper troposphere (200–500 hPa). Following Equation 1, tracer tendency is separated into contribution from deep convection (red, COND), shallow convection (orange, CONS), vertical diffusion (blue, VD), and transport by resolved dynamics (green, RD). From Equation 4, transport by resolved dynamics is further decomposed into zonal transport (crosshatched purple), meridional transport (crosshatched magenta), and vertical transport (crosshatched cyan). The residual of Equation 4 due to using daily mean data to estimate the rhs of the equation, is in yellow shadings (crosshatched). The budget analysis for different tracers is performed over 30°N–70°N with the same east-west boundary in Figure 3. Unit is (mol/mol)/day. (b) The same as (a), but for 500–950 hPa. (c and d) The same as (a and b), but for day 3–5. (e and f) The same as (a and b), but for day 6–8.

In the lower troposphere (second column in Figure 4), vertical diffusion contributes the most, while deep and shallow convections have little contribution. Since the tracers are released during day 1, the tracer concentration is high near the surface, creating a strong vertical gradient in tracer concentrations and thus vertical diffusion can effectively bring the tracers up from the surface to the lower troposphere during day 1–2 (Figure 4b). As the tracer concentration decreases at the surface after day 1, the vertical gradient of tracer concentration reverses, and vertical diffusion brings the tracers downward back to the surface (Figure 4d). Since deep convection can bring tracers from the surface up into the lower troposphere (net gain of tracer concentration in the lower troposphere), and also lift tracers from the lower troposphere into the upper troposphere (net loss of tracer concentration in the lower troposphere), it plays little role in the lower troposphere (Figures 4b and 4d). Shallow convection vertically redistributes the tracers within the lower troposphere. This vertical redistribution has little net contribution to the tracer concentration when averaged within the lower troposphere (500–950 hPa; Figures 4b, 4d, and 4f). Also note that when the tracers are released on day 1, a large vertical gradient of tracer concentration is created near the surface, which leads to a large upward flux due to the vertical motion near the surface. This is the reason that the vertical transport by large-scale ascent leads to a positive tracer tendency in both upper troposphere (Figure 4a) and lower troposphere (Figure 4b).

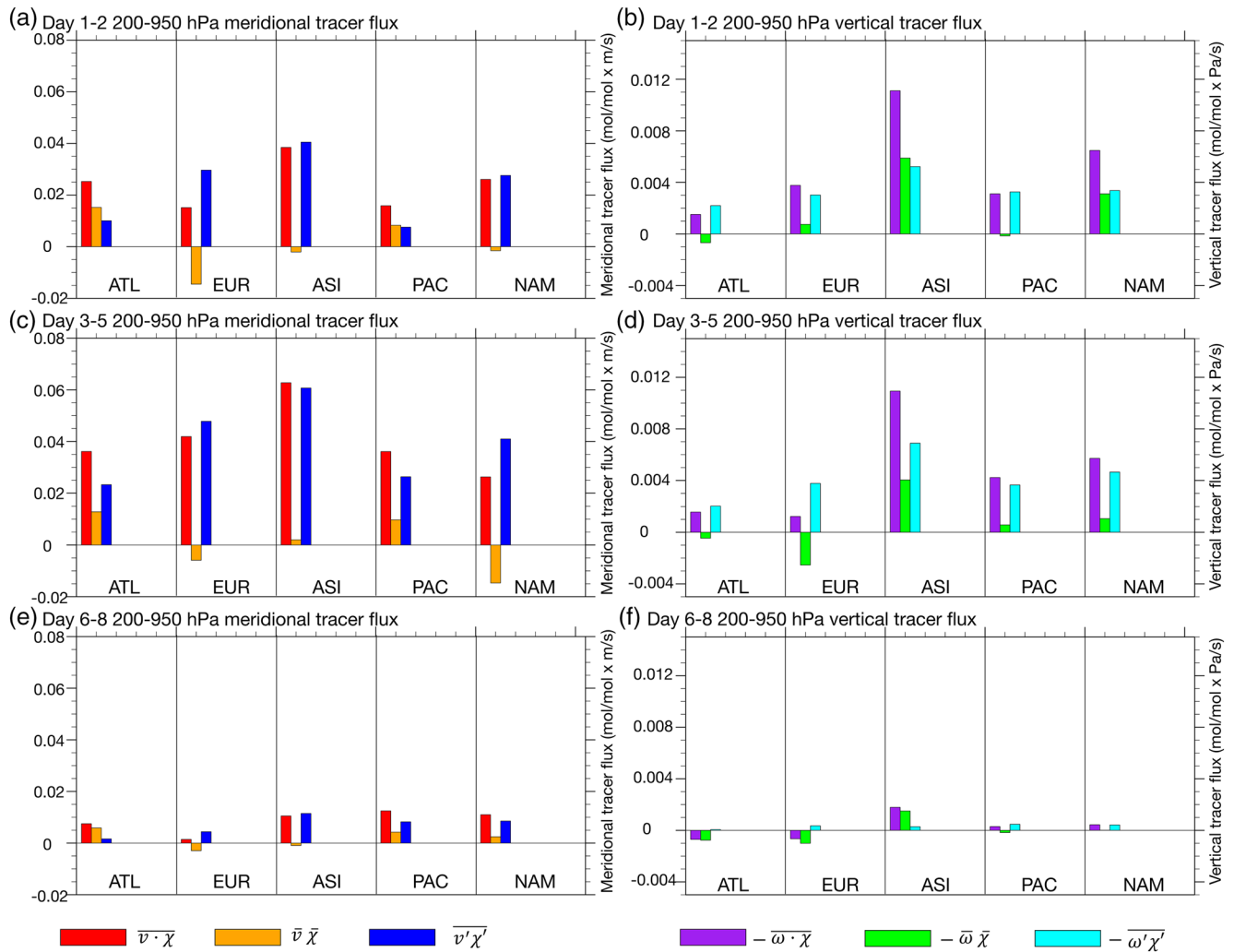


Figure 5. a) Decomposition of meridional tracer flux of different tracers during day 1–2 from 200 to 950 hPa. The decomposition of different tracers is performed over 50°N–70°N with the same east-west boundary in Figure 3. The total meridional flux is denoted by red, while the flux by climatological wind and transients is denoted by orange and blue respectively. Unit in $(\text{mol} / \text{mol}) \cdot (\text{m} / \text{s})$. (b) Similar to (a), but for the decomposition of vertical tracer flux by resolved dynamics over 30°N–70°N with the same east-west boundary in Figure 3. The total upward flux is denoted by purple, while the flux by climatological wind and transients is denoted by green and cyan, respectively. Unit in $(\text{mol} / \text{mol}) \cdot (\text{m} / \text{s})$. (c and d) The same as (a and b), but for day 3–5. (e and f) The same as (a and b) but for day 6–8. TP, Tibetan Plateau.

To explore the relative contributions of the time-mean and transient circulation to the meridional and vertical fluxes, we use Equations 5 and 6 to further decompose these fluxes. We analyze the meridional tracer flux averaged over 50°–70°N within the cross sections in Figure 3 for all five midlatitude regions. Note that generally the strongest meridional flux is located between 50° and 70°N (Figure 3), and the meridional flux at this latitude band is likely to contribute to the transport into the Arctic. Also, though here the analysis is within the entire troposphere (200–950 hPa), we reach similar conclusions regarding the time-mean and transient transport if upper and lower troposphere are analyzed separately (not shown). Note that, as transient wind is defined as deviation from time-mean wind during 10 years in Equations 5 and 6, transient transport includes contribution from variability on all different time scales (interannual, month-to-month, and sub-monthly). Our analysis shows that the transient transport is dominated by contribution from short time scale variability (sub-monthly; not shown). The decomposition of meridional flux (first column in Figure 5) shows that, consistently over the first 8 days, most of the northward flux is due to transients (blue) for EUR, ASI, and NAM tracers, while transport by time-mean wind (orange) and transients are both important for ATL and PAC tracers. The transport by time-mean wind, which is likely due to the northward

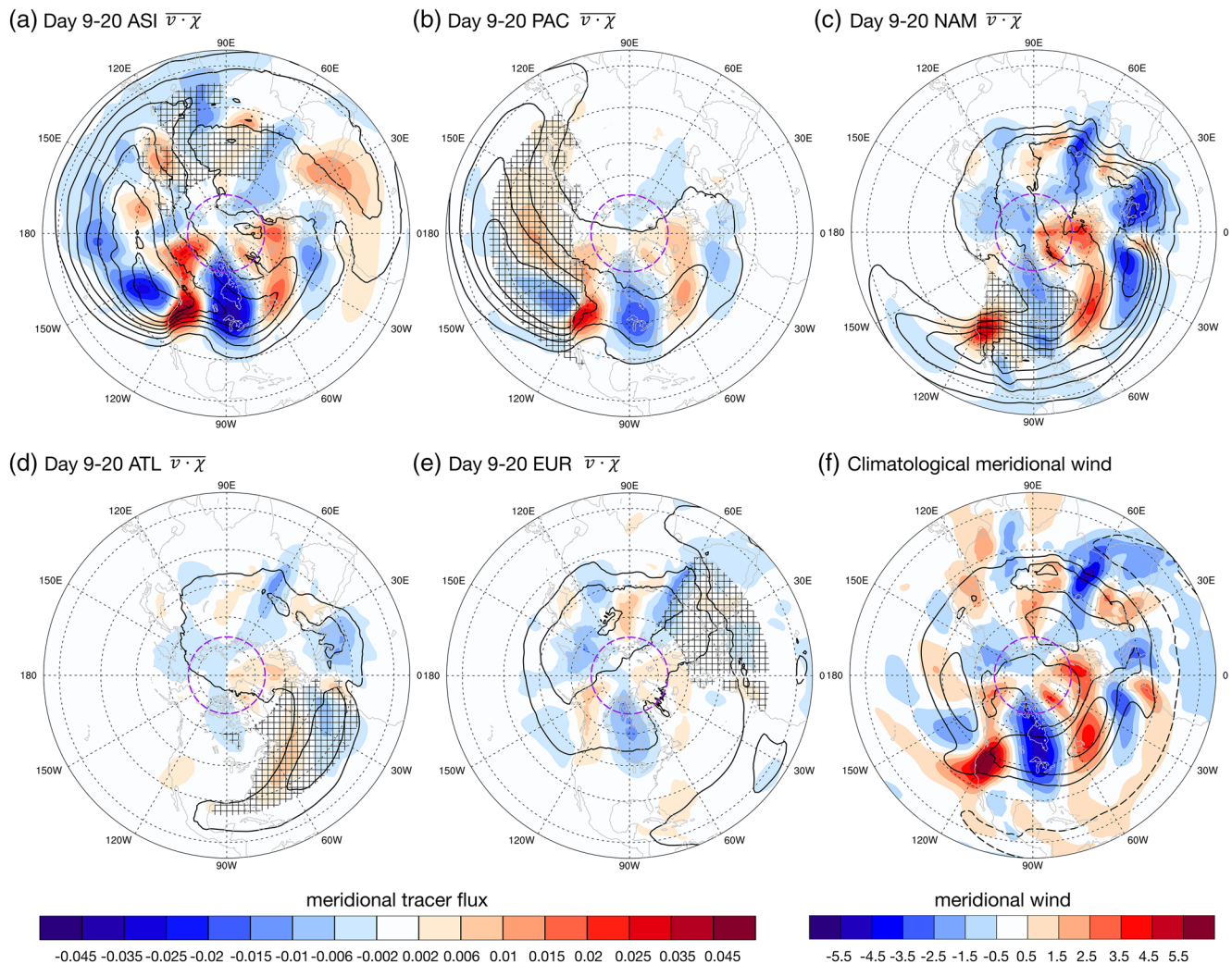


Figure 6. a) The shadings are the meridional tracer flux averaged vertically (1,000–100 hPa) during day 9–20 for ASI tracers. Unit in $(\text{mol} / \text{mol}) \cdot (\text{m} / \text{s})$. The black contours are the vertically averaged (1,000–100 hPa) tracer concentration. Contour interval is 0.0015 mol/mol. The boundary of Arctic region is denoted by the dashed purple line. The source region of the tracers is crosshatched. (b–e) The same as (a), but for PAC, NAM, ATL and EUR tracers respectively. (f) The shadings are the model July to August climatological meridional wind (1981–1990) averaged from 800 to 200 hPa. Unit in m/s. The contours are the climatological zonal wind at the same vertical levels during the same time period. Contour interval is 5 m/s. ASI, Asia; ATL, Atlantic; EUR, Europe; NAM, North America; PAC, Pacific.

transport near the exit of the Pacific and Atlantic jet, will be discussed in more detail in Section 4.3. The decomposition of vertical flux by resolved dynamics (second column in Figure 5), shows that transients (cyan) are important for tracers released in all five regions, with the time-mean vertical transport (green) also making a large contribution for ASI and NAM tracers.

In short, the fast transport pathway brings midlatitude tracers directly into the Arctic in both the lower and the upper troposphere within about 8 days. Vertical diffusion brings tracers up into the lower troposphere, while deep convection and resolved dynamics bring tracers into the upper troposphere. The poleward transport of the tracers into the Arctic is dominated by transients for Asian, European and North American tracers, while both time-mean and transient transports are important for poleward transport of Pacific and the Atlantic tracers.

4.3. The Intermediate Transport Pathway

Now, we investigate what circulation processes contribute to the intermediate time scale transport pathway. As discussed in Sections 3 and 4.1, during day 9–20 after the tracers are released, the meridional tracer

flux continues transporting ASI and PAC tracers into the Arctic substantially, which maintains or slightly increases the ASI and PAC tracer concentrations in the Arctic. On the contrary, the meridional tracer flux becomes southward for EUR and ATL tracers. To understand this, in Figures 6a–6e, the day 9–20 vertically integrated (1,000–100 hPa) meridional tracer flux (shadings) for ASI, PAC, NAM, ATL, and EUR tracers is shown respectively. The tracer concentration, which is also averaged vertically during day 9–20, is plotted in black contours. The source regions of tracers are cross-hatched in the map. In addition, the simulated July to August climatological wind, averaged from 800 to 200 hPa, is shown in Figure 6f, with meridional wind in shadings and zonal wind in contours, both comparing well with the observational reanalysis (not shown). Note that, as the goal here is to understand the transport into the Arctic, we will focus on the meridional transport in the high latitudes (around 50°–70°N). Details about tracer concentration and meridional flux in the mid-to-lower latitudes will not be discussed. The amplitude of meridional flux depends on the concentration of the tracers during day 9–20, while the concentration is determined by the amount of tracers released during day 1 and the amount of tracers removed throughout day 1–20. Since the amount of tracers that is released and removed from different source regions can be different, we do not focus on comparing the amplitude of concentration or meridional flux among different regions, but rather focus on what the favorable locations are for tracers to be transported into the Arctic.

In Figures 6a–6e, for tracers released in each source region, there are large tracer concentrations located downstream (eastward) of the source regions in the mid-to-high latitudes, consistent with zonal transport by the jet stream (Figure 6f) from days 9–20. The transport of tracers is westward in the subtropics and tropics. The downstream (eastward) long-range zonal transport of tracers from different emission regions (e.g., Asian, Europe and North America) has been investigated in previous studies by using both observations and model simulations (e.g., Akimoto, 2003; Chin et al., 2000; Duncan & Bey, 2004; Fang et al., 2009; Hudman et al., 2004; Huntrieser et al., 2005; Lewis et al., 2007; Q. Li et al., 2002; Liang et al., 2004). For ASI tracers (Figure 6a), the large tracer concentration extends from eastern north Pacific to North Atlantic, with strong northward flux into the Arctic located over Alaska and northern North Atlantic. Large tracer concentration is found over central to eastern North Pacific for PAC tracers, and part of the PAC tracers have also been transported into the northern North Atlantic (Figure 6b). The northward flux of PAC tracers into the Arctic is also located over Alaska and North Atlantic. Note that the distribution of meridional tracer transport (both northward and southward transport) for ASI and PAC tracers (Figures 6a and 6b) matches well with the distribution of the climatological meridional wind (Figure 6f). This suggests that Alaska and northern North Atlantic, where the climatological meridional wind is northward, are the favorable locations for tracers to be transported into the Arctic. Note that, the transport into the Arctic over these two regions (Alaska and northern North Atlantic) is not necessarily via the climatological wind only, since these two regions are also favorable for northward transport by transient eddies as they are located at the exit region of the Pacific and Atlantic storm tracks. Additional analysis shows that northward transport over the northern North Atlantic is dominated by contribution from climatological wind, while both climatological wind and transients are important for northward transport of PAC tracers over Alaska (Figure S1).

The distribution of the meridional flux for NAM, ATL, and EUR tracers (Figures 6c–6e), also corresponds well with the distribution of the climatological meridional wind (Figure 6f) except for a much weaker magnitude for ATL and EUR tracers compared to other tracers. For ATL and EUR tracers, a large proportion of the tracers is transported downstream into Eurasia. With climatological wind generally flowing southward over eastern Europe and western Siberia (around 60°E) as well as over eastern Siberia (around 150°E), the net meridional transport of tracers is southward for ATL and EUR tracers. Therefore, ATL and EUR tracers are not effectively transported into the Arctic during day 9–20. In Figure 6c, the NAM tracer is also transported into the North Atlantic where it is favorable for northward transport into the Arctic. This zonal transport can happen in relatively short time compared to ASI tracers being transported to the eastern North Pacific or PAC tracers to the North Atlantic, because of the closer proximity between North America and North Atlantic. Thus, the intermediate transport pathway can happen rather quickly for NAM tracers, which is the reason why the meridional flux into the Arctic is positive during the first 10 days for NAM tracers (Figure 2c). However, when the NAM tracers are transported further downstream into Europe, where the climatological flow is generally southward, the net meridional flux of NAM tracers turns negative. This explains why the NAM meridional tracer flux shifts to negative after 10 days (Figure 2c). The peak tracer concentration at 10 days for NAM tracers (Figures 1e and 1f), which is in between the peak time of ATL and

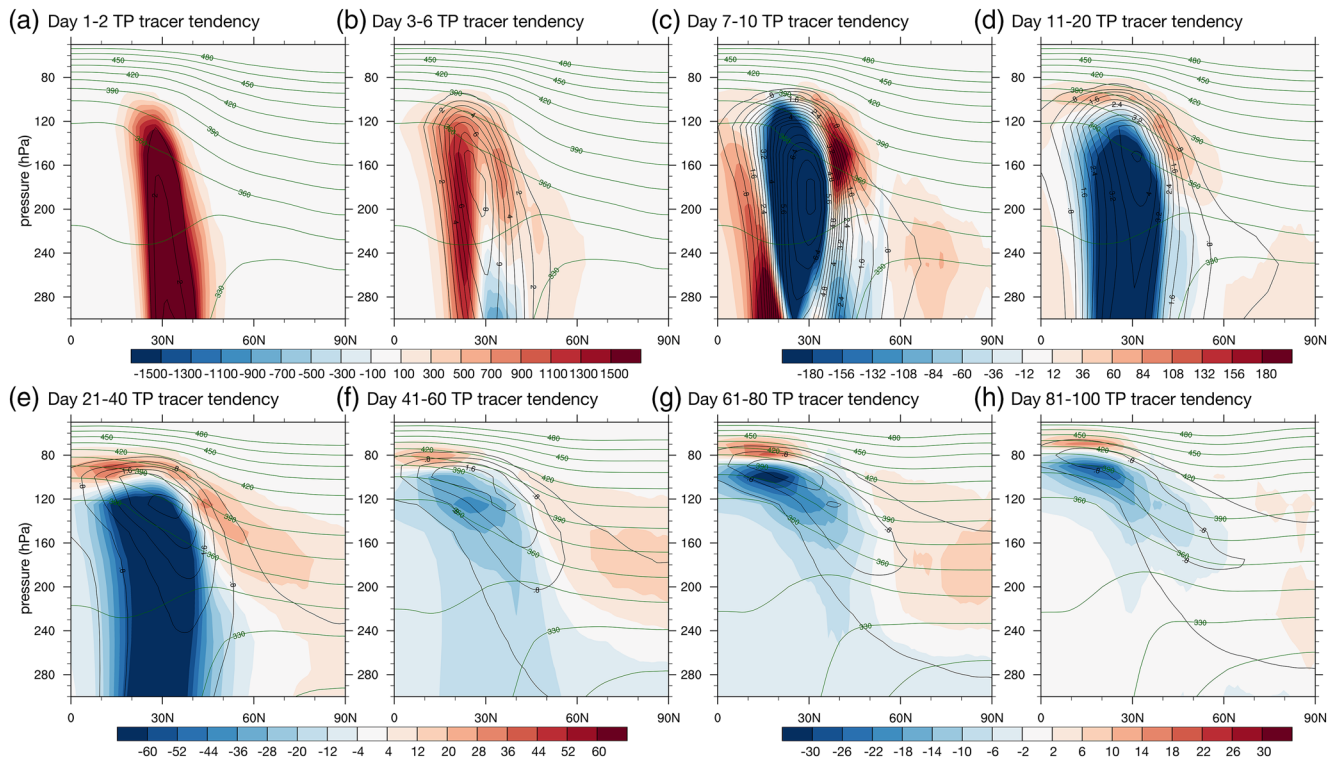


Figure 7. a) The shadings are zonally averaged tracer concentration tendency during day 1–2 for TP tracers. Unit in ppmv/day. The black contours are the zonally averaged tracer concentration. Contour interval is 0.5 millimole/mole. The green contours are the potential temperature levels. Contour interval is 15K. (b) The same as (a) but for day 3–6. (c–h) The same as (a), but for day 7–10, 11–20, 21–40, 41–60, 61–80, and 81–100, respectively. The tracer concentration contour (black) interval is 0.2 mmol/mol. TP, Tibetan Plateau.

EUR tracers (6–9 days), and ASI (10–30 days) and PAC tracers (10–15 days; see Figure 2), is due to the combination of the fast transport pathway and the intermediate transport pathway. The fact that climatological northward flow is located over Alaska and North Atlantic, rather than other regions around the Arctic, can be the main reason why both time-mean and transient transports are important for PAC and ATL tracers for the fast transport pathway, while transport by transients dominates for ASI, ATL and EUR tracers (Figures 5a, 5c, and 5e; also see Section 4.2 for more details).

Note that TP and NI tracers also show a concentration peak at around 40–60 days in the troposphere (Figures 1e and f), but with little contribution to the total Arctic tracer concentration (Figures 1b and 1c). Our analysis (not shown) suggests that the mechanism of this 40–60 days peak is similar to the intermediate transport pathway for midlatitude tracers discussed above. The TP/NI tracers are transported zonally by the jet first, and then can be transported into the Arctic over Alaska and the northern North Atlantic. However, as the source regions of TP and NI tracers are over the southern flank of the jet stream (Figure 6f), it takes longer time for these tracers to be transported to the northern flank of the jet where they can be transported into the Arctic. Whereas for midlatitude source regions, the majority of the tracers are already at the northern flank of the jet where they are released. Therefore, the intermediate transport pathway can happen much earlier for the midlatitude tracers than for subtropical tracers (TP and NI).

In short, during day 9–20, the tracers are transported downstream (eastward) by the zonal wind in the midlatitudes. ASI and PAC tracers are carried to Alaska and North Atlantic, and then transported into the Arctic, as these two locations are favorable for northward transport into the Arctic, leading to the intermediate transport timescales. However, as ATL and EUR tracers are advected downstream to Eurasia, where it is favorable for southward transport, they are not effectively transported into the Arctic during day 9–20, exhibiting no intermediate transport pathway. Note that our results that Alaska and North Atlantic are the favorable locations for northward transport into the Arctic, are in agreement with the model simulation re-

sults in previous studies (e.g., Akimoto, 2003; Hudman et al., 2004; Q. Li et al., 2002; Liang et al., 2004). The meridional transport pattern corresponds well with time-mean (decadal-mean) wind pattern, suggesting that low-frequency variability, which can lead to variability in the mean wind, can likely lead to interannual or decadal variability of the intermediate transport pathway.

4.4. The Slow Transport Pathway

We now examine the transport of tracers from tropical and subtropical regions (NI, TP, and TR) into the Arctic lower stratosphere, with the peak tracer concentration occurring at around 100 days. We will discuss the transport of TP tracers in detail as TP tracers are most efficiently transported into the Arctic among the three regions (Figure 1g). Later on, we will also show that the mechanism for NI and TR tracers is very similar to that for TP tracers.

The zonal mean tendency of TP tracers, from day 1 to 100, is shown in Figure 7. During the first few days after the tracers are released, the tendency of tracer concentration (Figures 7a and 7b, shadings) indicates that tracers are brought up effectively into the subtropical UTLS region. Subsequently, those tracers are transported both equatorward and poleward from the tracer concentration maximum in the subtropics (black contours; Figures 7b and 7c). From days 11–100 (Figures 7d–7h), a dipole pattern of the tracer tendency can be found in the UTLS in the tropics and subtropics, with a positive tendency above the tracer concentration maximum, and a negative tendency below, indicating a further upward lifting of the tracer concentration to about 80 hPa during day 81–100.

The growth of tracer concentration above the Arctic for TP tracers (Figure 1g) starts around days 20–30 after the tracers are released. The tendency of the tracers from day 21 to 100 shows a broad positive tendency over the midlatitude and polar lower stratosphere regions (Figures 7e–7h), with a larger tendency during day 21–60 (Figures 7e and 7f) than that during day 61–100 (Figures 7g and 7h; note the scale of Figures 7e–7h is different). It can be seen that the positive tendency over the midlatitude and polar regions can be traced back to the maximum tracer concentration near 120–70 hPa in the tropics and subtropics approximately following the isentropic surfaces (green contours). This suggests that the transport of tracers into the midlatitude and polar regions is likely through isentropic transport from the tropics and subtropics, when the large tracer concentration in the lower latitudes acts as a tracer reservoir.

So how are the tracers transported upward into the tropical and subtropical lower stratosphere? We first show the time scale of the vertical transport (Figure 8a) by displaying the time evolution of tracer concentration averaged over 0–40°N (also averaged zonally) at different pressure levels. The peak time of the concentration increases as a function of the vertical levels from about 5 days–120 days for pressure levels from 125 to 70 hPa. Thus, it takes on the order of 100 days to vertically transport tracers within the tropical and subtropical lower stratosphere.

The horizontal structure of the vertical transport in the lower latitudes is shown at 125, 100, 90, and 80 hPa (Figures 8b, 8c, 8f, and 8g). We plot the vertical fluxes of tracers (red for upward, blue for downward) averaged over 1–80 days, as the tracer concentration peaks at around 80 days for 80 hPa (Figure 8a). The vertical flux mostly happens from 10°E to 120°E in the subtropical region, with upward flux in the east and downward flux in the west. In addition to the vertical flux, the July to September modeled climatological vertical velocity is shown at the same pressure levels (Figures 8d, 8e, 8h, and 8i). Comparing the horizontal structure of vertical flux and vertical velocity (Figure 8b vs. Figure 8d, Figure 8c vs. Figure 8e, Figure 8f vs. Figure 8h, Figure 8g vs. Figure 8i), they are rather consistent. The area averaged (0°–40°N; 0–135°E) ascent, is about -5.1×10^{-4} Pa/s at 100 hPa and -2.7×10^{-4} Pa/s at 80 hPa. For an air mass to rise by 10 hPa, it takes about 23 days with the vertical velocity of -5.1×10^{-4} Pa/s (at 100 hPa), and about 43 days with the vertical velocity of -2.7×10^{-4} Pa/s (at 80 hPa). Consistent with Figure 8a, it takes about a month for TP tracers to rise by 10 hPa above the 100 hPa level.

For TP tracers, the vertical transport in the UTLS region is mostly due to the dipole structure of the vertical velocity from 10°E to 120°E, with upward motion in the east and downward motion in the west, which coherently exists at all 4 levels in Figure 8. This dipole structure of vertical motion, associated with the upper level anti-cyclone over the Asian summer monsoon region, has been documented by previous studies (e.g.,

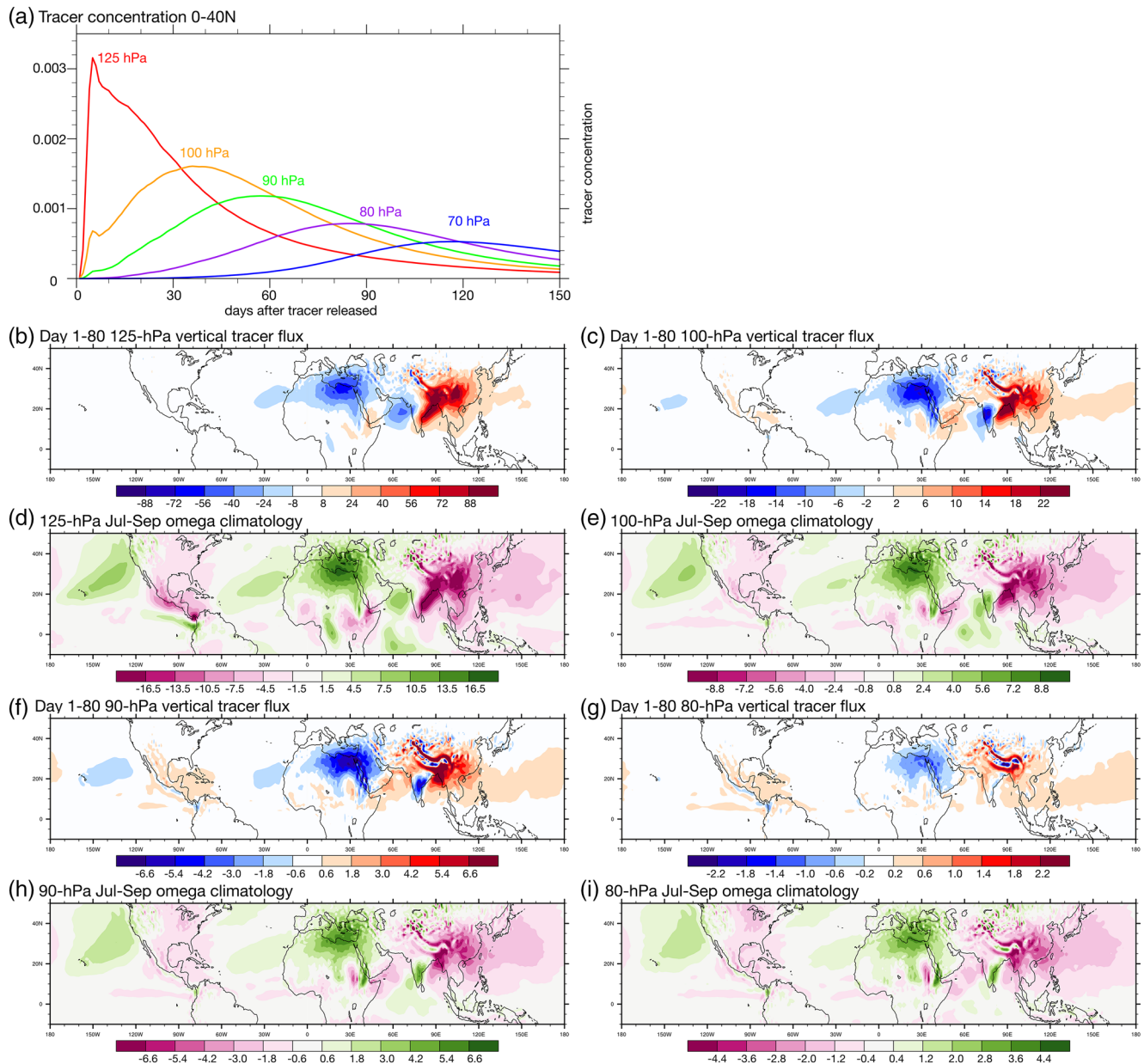


Figure 8. a) Temporal evolution of zonally averaged TP tracer concentration from 0 to 40°N for 125, 100, 90, 80, and 70 hPa. Unit in mol/mol. (b) Vertical tracer flux averaged during day 1–80 at 125 hPa (red for upward flux and blue for downward flux). Unit in $(\text{mol} / \text{mol}) \cdot (\text{m} / \text{s})$. (c) The same as (b) but for 100 hPa. (d) Model July to September climatological vertical velocity (1981–1990). Unit in Pa/s. (e) The same as (d) but for 100 hPa. (f and g) The same as (b), but for 90 and 80 hPa respectively. (h and i) The same as (d) but for 90 and 80 hPa, respectively. TP, Tibetan Plateau.

Bergman et al., 2013; Fu et al., 2006; C. Orbe, Newman et al., 2015; Pan et al., 2016; M. Park et al., 2009; Randel et al., 2010; Rodwell and Hoskins 1996, 2001; Tissier & Legras, 2016; Vogel et al., 2015, 2019). The strong rising motion directly above the source region of NI and TP tracers in the UTLS, is likely the reason why NI and TP tracers can be most efficiently transported into lower latitude UTLS (Figure 7a; also see Wu et al., 2020) and then into the Arctic (Figure 1g).

The transport pathway for NI and TR tracers is similar to TP tracers. The evolution of the tracer tendency (Figure S2 for NI and Figure S3 for TR), is similar to TP (Figure 7) as we see broad positive tendency over the midlatitude and polar lower stratosphere from day 21–100, which is at the same potential temperature levels as the maximum tracer concentration in the lower latitudes. Again, this implies isentropic transport from

the tropics into high latitudes. The vertical transport of tracers in the lower latitudes is shown in Figure S4 for NI and Figure S5 for TR. Consistent with TP tracer, the vertical tracer fluxes follow the climatological vertical velocity. Note that for TR tracers, upward transport in the lower stratosphere can happen both in the tropics and in the subtropical summer monsoon regions. Thus, TR tracers are not only lifted up locally, but also transported horizontally into regions favorable for upward transport and then brought up by the vertical motion.

5. Discussions and Conclusions

In this study, we investigate the summertime transport pathways from different surface regions in the NH into the Arctic by implementing and analyzing a large ensemble of idealized tagged tracers in WACCM5. Three different transport pathways have been identified by examining the temporal tracer concentration evolution in the Arctic. The fast transport pathway can bring tracers from all midlatitude regions into the Arctic within the troposphere on time scales less than 8 days. The intermediate transport pathway transports tracers released over Asia and Pacific into the Arctic in 9–20 days. The slow transport pathway brings tropical and subtropical tracers into the Arctic lower stratosphere in 1–3 months.

The fast transport pathway, which works efficiently for all the midlatitude regions, brings tracers directly to the north from the source region into the Arctic in both the upper and lower troposphere through meridional transport. The meridional and vertical processes relevant for the fast transport pathway is summarized in the schematic diagrams (Figures 9a and 9b). During the first 2 days after the tracers are released (Figure 9a), the tracers are lifted upward into the lower troposphere by vertical diffusion. Furthermore, tracers are also transported into the upper troposphere during the first 2 days by deep convection and transient vertical transport. Strong poleward transport locates in the lower troposphere at around 60°N, which is at the northern boundary of the source region. The northward transport in the upper troposphere is broader but weaker compared to that in the lower troposphere. During day 3–8 (Figure 9b), as the tracer concentration at the surface reduces due to surface deposition, vertical diffusion brings the tracers downward back to the surface in the lower troposphere. However, vertical transport by transients continues to bring tracers upward into the upper troposphere. The meridional transport into the Arctic is dominated by transients for tracers released in Asia, Europe and North America, while both time-mean and transient transports are important for tracers released in the Pacific and the Atlantic. Note that Yang et al. (2019) used a different framework to decompose the meridional transport of idealized tracers into zonal mean and zonally varying components, and they found both zonal mean and zonally varying components can be important for poleward transport. Here, we focus on the time-mean component and deviations from the time mean. The conclusions from different frameworks highlight the roles of different circulation features in transporting tracers poleward.

The intermediate transport pathway transports the tracers into the Arctic on the time scale of 1–3 weeks (Figure 9c). The tracers are first transported zonally by the jet stream. Then, if the tracers are transported into regions that are favorable for northward transport into the Arctic, which are over Alaska and the northern North Atlantic, then these tracers can be further transported into the Arctic. For tracers released in Asia and the Pacific, as the source regions are located upstream (west) of the favorable northward transport locations (Alaska and northern North Atlantic), tracers can be advected by the zonal jet and then efficiently transported into the Arctic via the intermediate transport pathway. However, for tracers released in Europe and the Atlantic, as the source regions are located downstream (east) of the two favorable northward transport locations, the zonal jet transports these tracers into locations (Eurasia) favorable for southward transport out of the Arctic. Thus, Europe and Atlantic tracers do not exhibit a clear intermediate transport pathway.

The fast and intermediate transport pathways have distinct features. The timescales of the transport are different, and the ways the tracers are transported horizontally are also different. The tracers are transported directly to the north via the fast transport pathway while they are first advected zonally before transported northward into the Arctic via the intermediate transport pathway. These are new findings that have not been documented by previous studies. In addition, we utilize a detailed budget analysis of tracer concentration as well as a decomposition analysis of the transport into time mean and transient components to understand the mechanism of the two pathways. This is also a novel aspect of this study.

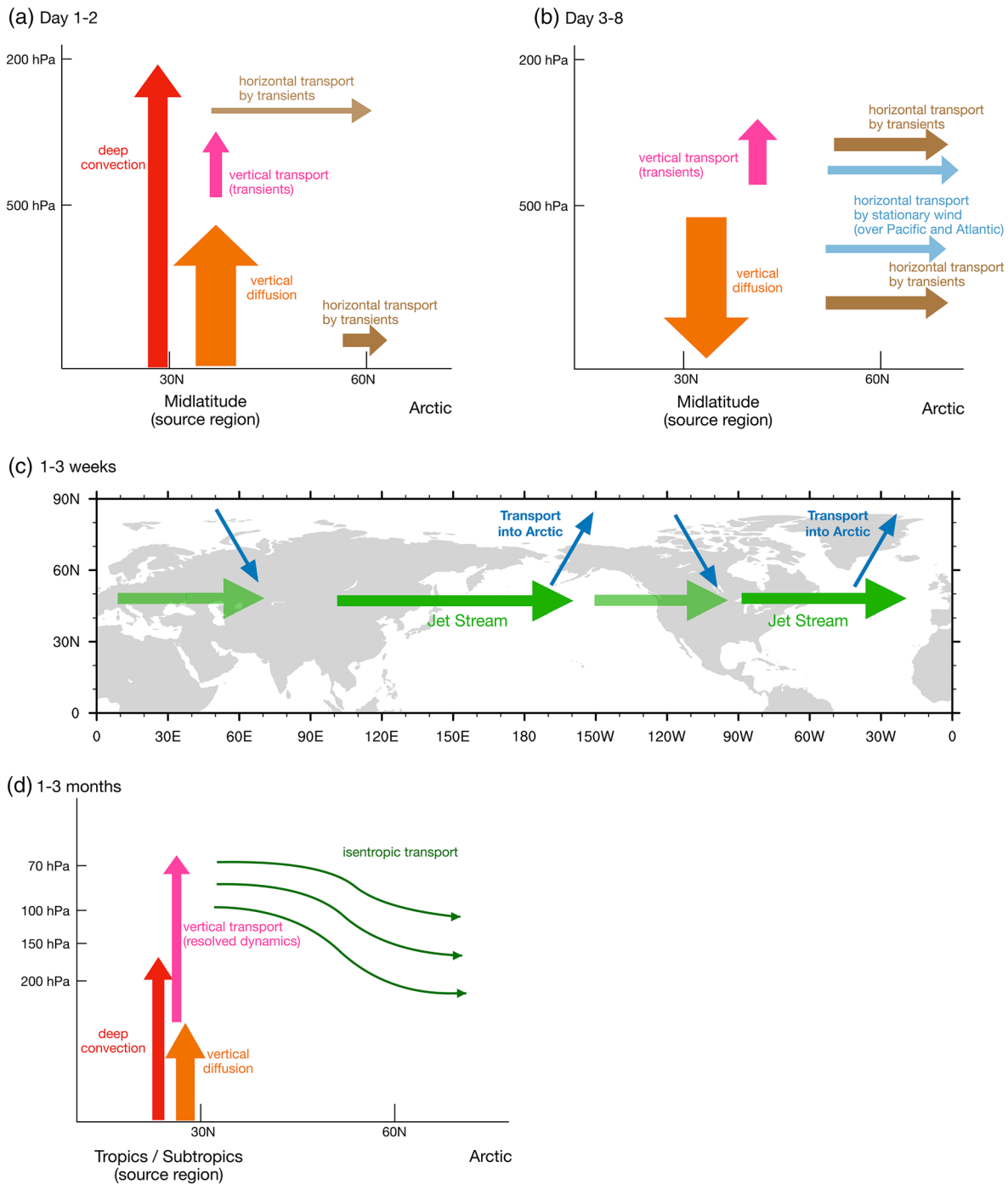


Figure 9. Schematic diagrams for different transport pathways. (a and b) The fast transport pathway. The width of the arrows indicates the relative importance of different processes. (c) The intermediate transport pathway. (d) The slow transport pathway.

The slow transport pathway carries the tropical and subtropical tracers into the Arctic lower stratosphere. A schematic diagram for the slow transport pathway is shown in Figure 9d. The tracers are first effectively brought up into the upper troposphere in the tropics and subtropics, mostly by deep convection and large-scale ascent. Then, the tracers are slowly transported upward into the lower stratosphere at locations where the climatological upward motion is prominent. These locations for upward transport into the lower stratosphere are not limited to the tropics, as strong vertical motion can also be found in the UTLS in the summer

monsoon regions. The transport pathway into the UTLS in the summer monsoon regions has been well documented by previous studies (e.g., Pan et al., 2016; M. Park et al., 2009; Randel et al., 2010 and others). The results from a few previous studies (e.g., Bourassa et al., 2012; Orbe et al., 2015) suggest that tracer species or aerosols can be transported to the Arctic after they are lifted up into the lower stratosphere over the summer monsoon region. Our study shows more details about this transport pathway and associated timescales. The tracers are first lifted up from 100 to 70 hPa over the monsoon region on 1–4 months' time scale, and they can then be transported into the midlatitude and the Arctic following the isentropes. As the climatological upward motion during summer is the strongest over the Asian monsoon region, tracers released in northern India and Tibetan Plateau, which are right beneath the upper level rising motion, can be most efficiently transported into the Arctic via the slow transport pathway.

In this study, we focus on understanding the main features of the three different transport pathways. These transport pathways can have month-to-month (e.g., July vs. August), interannual and decadal variabilities as the circulation pattern changes. Our preliminary analysis suggests that, as the circulation structure is not very different between July and August, the time scale and circulation processes involved in these pathways are similar, whereas the spatial pattern of the meridional transport for fast and intermediate can be slightly different (not shown). The slow transport pathway is slightly more efficient during July than August, which is likely because tracers are more efficiently transported into the UTLS over the Asian summer monsoon region during July as pointed out by Wu et al. (2020). The time-mean wind pattern can also be different during different years or decades due to low-frequency variability, suggesting that there could be substantial interannual or decadal variability for fast and intermediate transport pathways. The variability of Asian summer monsoon can also lead to interannual variability of the slow transport pathway. These topics are currently being explored and will be reported in future studies.

Consistent with C. Orbe, Newman et al. (2015a), our results indicate that midlatitude source regions contribute the most to the passive tracer concentration within the Arctic troposphere, whereas tropical and subtropical source regions contribute the most in the Arctic lower stratosphere. Our findings also suggest that pollutants emitted over all NH midlatitude land regions could be quickly transported into the Arctic troposphere within about one week via the fast transport pathway. Tracer species and aerosols emitted over Asia and North America could also be transported into the Arctic troposphere in about 1 to 3 weeks via the intermediate transport pathway. Regions like northern India and Tibetan Plateau are highlighted by the slow transport pathway and might have important implications for the transport of chemical species, such as ozone depleting substances, to the Arctic lower stratosphere. The approach with idealized tracers that have a spatially uniform source in this study focuses on the role of atmospheric dynamics underlying the transport pathways. To properly attribute the Arctic concentration of different chemical species to different source regions, the spatial distribution of emission (e.g., anthropogenic emission) needs to be taken into account. Future work will be devoted to linking the idealized tracer results to realistic emission sources and their implications.

Acknowledgments

The authors would like to thank Robert Fajber and two anonymous reviewers for comments that helped to improve this study. We acknowledge the support from National Science Foundation (NSF) Award OPP-1825858. Y. Wu also acknowledges the support from her startup fund from Lamont. Y. Wu and X. Wang are also supported by NSF Award AGS-1802248. We are grateful to Dr. Pengfei Zhang for his help in model setups. Computing and data storage resources, including the Cheyenne supercomputer, were provided by NCAR's Computational and Information Systems Laboratory, which is sponsored by NSF. X. Wang thanks William J. Randel and ASP program for allocations on Cheyenne.

Data Availability Statement

The data produced for and analyzed in this study is available through Columbia University Academic Commons (<https://academiccommons.columbia.edu/doi/10.7916/d8-9yp5-6p27>).

References

- Akimoto, H. (2003). Global air quality and pollution. *Science*, 302, 1716–1719. PMIS. <https://doi.org/10.1126/science.1092666>
- Atlas, E. L., Ridley, B. A., & Cantrell, C. A. (2003). The tropospheric ozone production about the spring equinox (TOPSE) experiment: Introduction. *Journal of Geophysical Research*, 108, 8353. <https://doi.org/10.1029/2002JD003172>
- Bergman, J. W., Fierli, F., Jensen, E. J., Honomichl, S., & Pan, L. L. (2013). Boundary layer sources for the Asian anticyclone: Regional contributions to a vertical conduit. *Journal of Geophysical Research: Atmosphere*, 118, 2560–2575. <https://doi.org/10.1002/jgrd.50142>
- Bond, T. C., Doherty, S. J., Fahey, D. W., Forster, P. M., Berntsen, T., DeAngelo, B. J., et al. (2013). Bounding the role of black carbon in the climate system: A scientific assessment. *Journal of Geophysical Research: Atmosphere*, 118, 5380–5552. <https://doi.org/10.1002/jgrd.50171>
- Bottenheim, J. W., Dastoor, A., Gong, S. L., Higuchi, K., & Li, Y. F. (2004). Long range transport of air pollution to the Arctic. In Handbook of environmental chemistry (Vol. 4G, pp. 13–39). Berlin, Heidelberg: Springer. <https://doi.org/10.1007/b94522>
- Bourassa, A. E., Robock, A., Randel, W. J., Deshler, T., Rieger, L. A., Lloyd, N. D., et al. (2012). Large volcanic aerosol load in the stratosphere linked to Asian monsoon transport. *Science*, 337(6090), 78–81. <https://doi.org/10.1126/science.1219371>

- Chin, M., Rood, R. B., Lin, S.-J., Müller, J.-F., & Thompson, A. M. (2000). Atmospheric sulfur cycle simulated in the global model GOCART: Model description and global properties. *Journal of Geophysical Research*, *105*, 24671–24687. <https://doi.org/10.1029/2000JD900384>
- Coopman, Q., Garrett, T. J., Finch, D. P., & Riedi, J. (2018). High sensitivity of Arctic liquid clouds to long-range anthropogenic aerosol transport. *Geophysical Research Letters*, *45*, 372–381. <https://doi.org/10.1002/2017GL075795>
- Duncan, B. N., & Bey, I. (2004). A modeling study of the export pathways of pollution from Europe: Seasonal and interannual variations (1987–1997). *Journal of Geophysical Research*, *109*, D08301. <https://doi.org/10.1029/2003JD004079>
- Fang, Y., Fiore, A. M., Horowitz, L. W., Gnanadesikan, A., Levy, H., Hu, Y., & Russell, A. G. (2009). Estimating the contribution of strong daily export events to total pollutant export from the United States in summer. *Journal of Geophysical Research*, *114*, D23302. <https://doi.org/10.1029/2008JD010946>
- Fisher, J. A., Jacob, D. J., Purdy, M. T., Kopacz, M., Le Sager, P., Carouge, C., et al. (2010). Source attribution and interannual variability of Arctic pollution in spring constrained by aircraft (ARCTAS, ARCPAC) and satellite (AIRS) observations of carbon monoxide. *Atmospheric Chemistry and Physics*, *10*, 977–996. <https://doi.org/10.5194/acp-10-977-2010>
- Fu, R., Hu, Y., Wright, J. S., Jiang, J. H., Dickinson, R. E., Chen, M., et al. (2006). Short circuit of water vapor and polluted air to the global stratosphere by convective transport over the Tibetan Plateau. *Proceedings of the National Academy of Sciences of the United States of America*, *103*(15), 5664–5669. <https://doi.org/10.1073/pnas.0601584103>
- Garcia, R. R., & Richter, J. H. (2019). On the momentum budget of the quasi-biennial oscillation in the whole atmosphere community climate model. *Journal of the Atmospheric Sciences*, *76*, 69–87. <https://doi.org/10.1175/JASD-18-0088.1>
- Garrett, T. J., & Zhao, C. (2006). Increased Arctic cloud longwave emissivity associated with pollution from mid-latitudes. *Nature*, *440*, 787–789. <https://doi.org/10.1038/nature04636>
- Haine, T. W. N., Zhang, H., Waugh, D. W., & Holzer, M. (2008). On transit-time distributions in unsteady circulation models. *Ocean Modelling*, *21*(1–2), 35–45.
- Hansen, J., & Nazarenko, L. (2004). Soot climate forcing via snow and ice albedos. *Proceedings of the National Academy of Sciences of the United States of America*, *101*, 423–428. <https://doi.org/10.1073/pnas.2237157100>
- Holzer, M., & Hall, T. M. (2000). Transit-time and tracer-age distributions in geophysical flows. *Journal of the Atmospheric Sciences*, *57*, 3539–3558.
- Holzer, M., McKendry, I. G., & Jaffe, D. A. (2003). Springtime trans-Pacific atmospheric transport from east Asia: A transit-time probability density function approach. *Journal of Geophysical Research*, *108*(D22), 47. <https://doi.org/10.1029/2003JD003558>
- Hudman, R. C., Jacob, D. J., Cooper, O. R., Evans, M. J., Heald, C. L., Park, R. J., et al. (2004). Ozone production in transpacific Asian pollution plumes and implications for ozone air quality in California. *Journal of Geophysical Research*, *109*, D23S10. <https://doi.org/10.1029/2004JD004974>
- Huntrieser, H., Heland, J., Schlager, H., Forster, C., Stohl, A., Aufmhoff, H., et al. (2005). Intercontinental air pollution transport from North America to Europe: Experimental evidence from airborne measurements and surface observations. *Journal of Geophysical Research*, *110*, D01305. <https://doi.org/10.1029/2004JD005045>
- Hurrell, J. W., Holland, M. M., Gent, P. R., Ghan, S., Kay, J. E., Kushner, P. J., et al. (2013). The community earth system model: A framework for collaborative research. *Bulletin of the American Meteorological Society*, *94*, 1339–1360. <https://doi.org/10.1175/BAMS-D-12-00121.1>
- Ikedo, K., Tanimoto, H., Sugita, T., Akiyoshi, H., Kanaya, Y., Zhu, C., & Taketani, F. (2017). Tagged tracer simulations of black carbon in the arctic: Transport, source contributions, and budget. *Atmospheric Chemistry and Physics*, *17*(17), 10515–10533.
- Klonecki, A., Hess, P., Emmons, L., Smith, L., Orlando, J., & Blake, D. (2003). Seasonal changes in the transport of pollutants into the Arctic troposphere-model study. *Journal of Geophysical Research*, *108*, 8367. <https://doi.org/10.1029/2002JD002199>
- Koch, D., & Hansen, J. (2005). Distant origins of Arctic black carbon: AGoddard Institute for Space Studies ModelE experiment. *Journal of Geophysical Research*, *110*, D04204. <https://doi.org/10.1029/2004JD005296>
- Krishnamurti, T. N., Krishnamurti, R., Das, S., Kumar, V., Jayakumar, A., & Simon, A. (2015). A pathway connecting the monsoonal heating to the rapid Arctic ice melt. *Journal of the Atmospheric Sciences*, *72*, 5–34. <https://doi.org/10.1175/JAS-D-14-0004.1>
- Kupiszewski, P., Leck, C., Tjernström, M., Sjogren, S., Sedlar, J., Graus, M., et al. (2013). Vertical profiling of aerosol particles and trace gases over the central Arctic Ocean during summer. *Atmospheric Chemistry and Physics*, *13*, 12405–12431. <https://doi.org/10.5194/acp-13-12405-2013>
- Laliberte, F., & Kushner, P. J. (2014). Midlatitude moisture contribution to recent Arctic tropospheric summertime variability. *Journal of Climate*, *27*, 5693–5707. <https://doi.org/10.1175/JCLI-D-13-00721.1>
- Law, K. S., & Stohl, A. (2007). Arctic air pollution: Origins and impacts. *Science*, *315*, 1537–1540. <https://doi.org/10.1126/science.1137695>
- Lewis, A., Evans, M. J., Methven, J., Watson, N., Lee, J. D., Hopkins, J. R., et al. (2007). Chemical composition observed over the mid-Atlantic and the detection of pollution signatures far from source regions. *Journal of Geophysical Research*, *112*, D10S39. <https://doi.org/10.1029/2006JD007584>
- Liang, Q., Jaeglé, L., Jaffe, D. A., Weiss-Penzias, P., Heckman, A., & Snow, J. A. (2004). Long-range transport of Asian pollution to the north-east Pacific: Seasonal variations and transport pathways of carbon monoxide. *Journal of Geophysical Research*, *109*, D23S07. <https://doi.org/10.1029/2003JD004402>
- Li, Q., Jacob, D. J., Bey, I., Palmer, P. I., Duncan, B. N., Field, B. D., et al. (2007). Transatlantic transport of pollution and its effects on surface ozone in Europe and North America. *Journal of Geophysical Research*, *107*(D13), 4166. <https://doi.org/10.1029/2001JD001422>
- Li, F., Waugh, D. W., Douglass, A. R., Newman, P. A., Pawson, S., Stolarski, R. S., et al. (2012). Seasonal variations of stratospheric age spectra in the goddard earth observing system chemistry climate model (GEOSCCM). *Journal of Geophysical Research*, *117*, D05134. <https://doi.org/10.1029/2011JD016877>
- Liu, H., Jacob, D. J., Bey, I., Yantosca, R. M., Duncan, B. N., & Sachse, G. W. (2003). Transport pathways for Asian pollution outflow over the Pacific: Interannual and seasonal variations. *Journal of Geophysical Research*, *108*(D20), 8786. <https://doi.org/10.1029/2002JD003102>
- Liu, D., Quennehen, B., Darbyshire, E., Allan, J. D., Williams, P. I., Taylor, J. W., et al. (2015). The importance of Asia as a source of black carbon to the European Arctic during springtime 2013. *Atmospheric Chemistry and Physics*, *15*, 11537–11555. <https://doi.org/10.5194/acp-15-11537-2015>
- Lubin, D., & Vogelmann, A. M. (2006). A climatologically significant aerosol longwave indirect effect in the Arctic. *Nature*, *439*, 453–456. <https://doi.org/10.1038/nature04449>
- Neale, R. B., Chen, C.-C., Gettelman, A., Lauritzen, P. H., Park, S., Williamson, D. L., et al. (2010). *Description of the NCAR community atmosphere model (CAM 5.0)*. NCAR Technical Note NCAR/TN-486+STR.
- Orbe, C., Holzer, M., & Polvani, L. M. (2012). Flux distributions as robust diagnostics of stratosphere-troposphere exchange. *Journal of Geophysical Research*, *117*, D01302. <https://doi.org/10.1029/2011JD016455>

- Orbe, C., Newman, P. A., Waugh, D. W., Holzer, M., Oman, L. D., Li, F., & Polvani, L. M. (2015a). Airmass origin in the Arctic. Part I: Seasonality. *Journal of Climate*, *28*, 4997–5014. <https://doi.org/10.1175/JCLI-D-14-00720.1>
- Orbe, C., Waugh, D. W., & Newman, P. A. (2015b). Air-mass origin in the tropical lower stratosphere: The influence of Asian boundary layer air. *Geophysical Research Letters*, *42*(10), 4240–4248.
- Orbe, C., Waugh, D. W., Newman, P. A., & Steenrod, S. (2016). The transit-time distribution from the Northern Hemisphere midlatitude surface. *Journal of the Atmospheric Sciences*, *73*, 3785–3802.
- Pan, L. L., Honomichl, S. B., Kinnison, D. E., Abalos, M., Randel, W. J., Bergman, J. W., & Bian, J. (2016). Transport of chemical tracers from the boundary layer to stratosphere associated with the dynamics of the Asian summer monsoon. *Journal of Geophysical Research: Atmosphere*, *121*, 14159–14174. <https://doi.org/10.1002/2016JD025616>
- Park, M., Randel, W. J., Emmons, L., & Livesey, N. (2009). Transport pathways of carbon monoxide in the Asian summer monsoon diagnosed from model of ozone and related tracers (MOZART). *Journal of Geophysical Research*, *114*, D08303. <https://doi.org/10.1029/2008JD010621>
- Park, S., & Bretherton, C. S. (2009). The University of Washington shallow convection and moist turbulence schemes and their impact on climate simulations with the community atmosphere model. *Journal of Climate*, *22*, 3449–3469. <https://doi.org/10.1175/2008JCLI2557.1>
- Ploeger, F., & Birner, T. (2016). Seasonal and inter-annual variability of lower stratospheric age of air spectra. *Atmospheric Chemistry and Physics*, *16*, 10195. <https://doi.org/10.5194/acp-16-10195-2016>
- Quinn, P. K., Shaw, G., Andrews, E., Dutton, E. G., Ruoho-Airola, T., & Gong, S. L. (2007). Arctic haze: Current trends and knowledge gaps. *Tellus B: Chemical and Physical Meteorology*, *59*(1), 99–114. <https://doi.org/10.1111/j.1600-0889.2006.00236.x>
- Rahn, K. A., & McCaffrey, R. J. (1980). On the origin and transport of the winter Arctic aerosol. *Annals of the New York Academy of Sciences*, *338*, 486–503. <https://doi.org/10.1111/j.1749-6632.1980.tb17142.x>
- Randel, W. J., Park, M., Emmons, L., Kinnison, D., Bernath, P., Walker, K., et al. (2010). Asian monsoon transport of pollution to the stratosphere. *Science*, *328*, 611. <https://doi.org/10.1126/science.1182274>
- Rodwell, M. J., & Hoskins, B. J. (1996). Monsoons and the dynamics of deserts. *Quarterly Journal of the Royal Meteorological Society*, *122*, 1385–1404. <https://doi.org/10.1002/qj.49712253408>
- Rodwell, M. J., & Hoskins, B. J. (2001). Subtropical anticyclones and summer monsoons. *Journal of Climate*, *14*, 3192–3211. <https://doi.org/10.1002/qj.49712253408>
- Shindell, D. (2007). Local and remote contributions to Arctic warming. *Geophysical Research Letters*, *34*, 1–5. <https://doi.org/10.1029/2007GL030221>
- Shindell, D., Chin, M., Dentener, F., Doherty, R. M., Faluvegi, G., Fiore, A. M. et al. (2008). A multi-model assessment of pollution transport to the Arctic. *Atmospheric Chemistry and Physics*, *8*, 5353–5372. <https://doi.org/10.5194/acp-8-5353-2008>
- Stohl, A. (2006). Characteristics of atmospheric transport into the Arctic troposphere. *Journal of Geophysical Research*, *111*, D11306. <https://doi.org/10.1029/2005JD006888>
- Tissier, A.-S., & Legras, B. (2016). Convective sources of trajectories traversing the tropical tropopause layer. *Atmospheric Chemistry and Physics*, *16*, 3383–3398. <https://doi.org/10.5194/acp-16-3383-2016>
- Vogel, B., Günther, G., Müller, R., Groöß, J.-U., & Riese, M. (2015). Impact of different Asian source regions on the composition of the Asian monsoon anticyclone and of the extratropical lowermost stratosphere. *Atmospheric Chemistry and Physics*, *15*, 13699–13716. <https://doi.org/10.5194/acp-15-13699-2015>
- Vogel, B. R. M., Günther, G., Spang, R., Hanumanthu, S., Li, D., et al. (2019). Lagrangian simulations of the transport of young air masses to the top of the Asian monsoon anticyclone and into the tropical pipe. *Atmospheric Chemistry and Physics*, *19*, 6007–6034. <https://doi.org/10.5194/acp-19-6007-2019>
- Wang, X., Wu, Y., Tung, W.-W., Richter, J. H., Glanville, A. A., Tilmes, S., et al. (2018). The simulation of stratospheric water vapor over the Asian summer monsoon region in CESM1(WACCM) models. *Journal of Geophysical Research: Atmosphere*, *123*, 11377–11391. <https://doi.org/10.1029/2018JD028971>
- Warren, S. G., & Wiscombe, W. J. (1980). A model for the spectral albedo of snow. II: Snow containing atmospheric aerosols. *Journal of the Atmospheric Sciences*, *37*, 2734–2745. [https://doi.org/10.1175/1520-0469\(1980\)037<2734:AMFTSA>2.0.CO;2](https://doi.org/10.1175/1520-0469(1980)037<2734:AMFTSA>2.0.CO;2)
- Wu, Y., Orbe, C., Tilmes, S., Abalos, M., & Wang, X. (2020). Fast transport pathways into the Northern Hemisphere upper troposphere and lower stratosphere during northern summer. *Journal of Geophysical Research: Atmosphere*, *125*, e2019JD031552. <https://doi.org/10.1029/2019JD031552>
- Xu, J.-W., Martin, R. V., Morrow, A., Sharma, S., Huang, L., Leaitch, W. R., et al. (2017). Source attribution of Arctic black carbon constrained by aircraft and surface measurements. *Atmospheric Chemistry and Physics*, *17*, 11971–11989. <https://doi.org/10.5194/acp-17-11971-2017>
- Yang, H., Waugh, D. W., Orbe, C., Zeng, G., Morgenstern, O., Kinnison, D. E., & Schofield, R. (2019). Large-scale transport into the Arctic: The roles of the midlatitude jet and the Hadley Cell. *Atmospheric Chemistry and Physics*, *19*(8), 5511–5528. <https://doi.org/10.5194/acp-2018-841>
- Zhang, G. J., & McFarlane, N. A. (1995). Sensitivity of climate simulations to the parameterization of cumulus convection in the Canadian climate centre general circulation model. *Atmosphere-Ocean*, *33*, 407–446.